EFFECTS OF ALENDRONATE-IMMOBILIZED CALCIUM PHOSPHATE COATING ON BONE GROWTH INTO POROUS TANTALUM

—A GAP MODEL ANIMAL STUDY

by

YOUXIN HU

M.A.Sc. in Materials Science & Engineering, Northeast Univ. of Tech. China, 1990

B.A.Sc. in Materials Science & Engineering, Northeast Univ. of Tech. China, 1985

A THESIS SUBMITTED IN PARTIAL FULFILLMENT OF
THE REQUIREMENTS FOR THE DEGREE OF

MASTER OF APPLIED SCIENCE

in

THE FACULTY OF GRADUATE STUDIES

(Materials Engineering)

THE UNIVERSITY OF BRITISH COLUMBIA

April 2007

ABSTRACT

Porous tantalum has been shown to be a promising orthopaedic implant material because of its similarity to bone in both mechanical properties and its three-dimensional porous structure. However, in some circumstances, bone quality or quantity is insufficient to allow adequate bone ingrowth. Alendronate, one of the bisphosphonate families, affects the activities of bone cells and enhances bone formation. In this thesis, we hypothesized that the addition of alendronate could increase the osteoconductivity and bone-ingrowth of porous tantalum and overcome the challenges of bone-implant gaps.

To facilitate local delivery of alendronate, a micro-porous calcium phosphate coating was deposited onto the tantalum surface by an electrolytic deposition technique, which was followed by alendronate adsorption. Coating structures and morphologies were confirmed by scanning electron microscopy, X-ray diffraction, and Fourier transform infrared spectroscopy. The presence of alendronate was confirmed by high performance liquid chromatography.

To study the effects of alendronate-immobilized calcium phosphate coating on bone reaction to porous implants, an animal gap model, with a fixed gap of 0.6 mm between implants and bone, was developed. Three types of surfaces, which were non-coating (Ta), calcium phosphate coating (Ta-CaP), and alendronate-immobilized calcium phosphate coating (Ta-CaP-AlN), were compared. Two fluorochromes were adopted to track the front of bone formation. After four weeks of healing and following standard histology techniques, the implants were analyzed with backscattered electron microscopy and fluorescent optical microscopy for bone-implant interactions.

The relative volume increase of gap filling, bone ingrowth and total bone formation were 124 % (2.24-fold), 232% (3.32-fold) and 170% (2.7-fold) respectively in Ta-CaP-ALN compared with Ta controls. The contact length of newly formed bone on porous tantalum was increased by 700% (8-fold) in Ta-CaP-ALN compared with Ta plugs, suggesting enhanced osteoconductivity of Ta-CaP-ALN implants. The bone formation mechanism analysis found that bone growth initiated on both surfaces of the Ta-CaP-ALN implants and host bone, while little bone initiation on the Ta implant surface was detected. These significant enhancements of Ta-CaP-ALN may have direct applications in orthopaedics. For revision arthroplasty with insufficient bone stock, the local delivery of alendronate would enhance biological fixation of the implant and promote the healing of bone defects.

TABLE OF CONTENTS

LIST OF TABLES

LIST OF FIGURES

LIST OF ABBREVIATION

ALN	Alendronate
BMP	Bone morphogenic protein
BPP	Bisphosphonate
BSE	Backscattered Electron imaging
CaP	Calcium phosphate
DCPD	Dicalcium phosphate dihydrate
ECD	Electrochemical deposition
EDS	Energy dispersive spectrometry
ELD	Electrolytic deposition
FTIR	Fourier transform infrared spectroscopy
HA	Hydroxyapatite
HLPC	High performance liquid chromatography
OCP	Octacalcium phosphate
PMMA	Polymethymethacrylate
SD	Standard deviation
SEM	Scanning electron microscopy
Ta	Tantalum
Ta-CaP	Calcium-phosphate-coated porous tantalum
Ta-CaP-ALN	Alendronate-immobilized calcium-phosphate-coated porous tantalum
TCP	Tricalcium phosphate
THR	Total hip replacement
XRD	X-ray diffraction

ACKNOWLEDGMENTS

I would like to thank my supervisor, Dr. Rizhi Wang for his guidance during my research work, and Dr. Don Garbuz for supervising surgical protocols during animal tests.

I also would like to thank my colleagues, Ke Duan for his help throughout the entire project; Dr. Winston Kim for his excellent work on implant surgeries; Dr. Tom Oxland, Bas Masri and Clive Duncan for support in surgery designs; and Allen Tang for his support in biomaterial laboratory and in the Jack Bell Centre of the Vancouver General Hospital.

I would like to extend my thanks to Dr. Helen Burt and Mr. John Jackson in the Pharmaceutical Science Department of UBC; Ms. Mary Mager and other staff in the Materials Engineering Department of UBC and the animal care team at Jack Bell Centre in VGH.

Finally, Zimmer Inc. and NSERC, thank you for your support with the project.

CHAPTER 1: INTRODUCTION

Osteoporosis and osteoarthritis may cause severe damage to the hip and/or knee joints. Injuries occurring during sports and exercises may also break the femoral necks or the knee patellae. To treat these diseases and traumas, orthopaedists often have to replace the failed hip or knee joints with artificial ones made of metals, polymers or ceramics. Women are more vulnerable to osteoporosis [1]. After menopause a woman can lose up to 20% bone mass in 5 to 10 years [2], and this may cause brittleness of bone.

In the year 2004 – 2005, statistics showed that the number of knee replacements in Canada reached 33.6 thousand, which was an increase of 125% from the year 1994-1995, Tab 1.1. Also in 2005, hip replacements in Canada reached 25 thousand, an increase of 52% and 6% compared with years 1994 -1995 and 2003 – 2004 respectively [3]. Considering that the population of Canada in 2005 was 30 millions, almost two in every thousand Canadians have had either a hip or knee replacement in every year for the past 10 years. Therefore, any improvement in knee or hip replacements will significantly contribute to the Canadian health care system and dramatically benefit Canadian society.

Table 1. 1 Total numbers of hip and knee replacement procedures, Canada [3]

	1994–1995	2003–2004	2004–2005	10-year % Change	1-Year % Change
Knee Replacements	14,938	29,848	33,590	125%	13%
Hip Replacements	16,525	23,669	25,124	52%	6%
Total Replacements	31,463	53,517	58,714	87%	10%

Currently, poor fixation and unacceptably high revision rates are the major problems with knee and hip joint replacements. Poor early bone/implant integration, stress shielding and aseptic loosening are the major causes of failure of joint replacement implants [4, 5], and the longevity of these joint implants is 15 to 20 years. With the extension of human lifespan to 80 or 85 years in the 21st century, a revision joint arthroplasty may be needed. Therefore, enhancing the bone/implant fixation and reducing the revision rates of joint replacements remain the primary topics in orthopaedic research. In addition, the management of bone stock deficiency and the achievement of reliable and durable implant/host-bone fixation remain significant challenges in revision joint replacements.

The concept of a drug-implant delivery system in reconstructive orthopaedics was well established [6]. Bisphosphonates have been investigated as a means to promote early bone ingrowth [7, 8, 9]. Recently, an investigation of a canine model where a third generation bisphosphonate, zoledronic acid, bound to hydroxyapatite-coated porous tantalum implants demonstrated an increase in peri-implant bone growth within the intramedullary canal and a 58% increase in the bone ingrowth within the porous tantalum[10].

Laboratory experimental models should replicate clinical scenarios as closely as possible. In revision hip arthroplasty, host bone deficiencies, gaps and defects between implant and host bone are frequently encountered. Gaps as small as 50 to 500μm failed to be bridged by new bone in a study of human host bone and hydroxyapatite-coated implants [11]. The design of implant materials has to face challenges of the inevitable gaps between bone

and implants during arthroplasty surgeries, and the gap model animal tests are necessary for examining new designed implant materials.

Although the promising results on bisphosphonate-delivery implants were reported [10], the effects of bisphosphonate-immobilized calcium-phosphate coating on the location, pattern and extent of bone formation in the presence of a gap have not been previously investigated. We conducted a gap model animal study on alendronate-immobilized calcium-phosphate-coated porous tantalum implants. The calcium phosphate coatings we processed via electrolytic deposition were porous at 1 micrometer level, and the porous morphology was good for bisphosphonate immobilization. Low concentration (less than 10^{-4} mol/l) of alendronate, which was one of the bisphosphonate families, was immobilized on the surfaces of ELD calcium phosphate coating. We hypothesized that the alendronate-immobilized calcium phosphate coating could increase the osteoconductivity and bone ingrowth of porous tantalum implants and therefore enhance the peri-prosthetic bone growth. Eventually, better bone/implant fixation could be achieved.

The purpose of this study was (1) to develop an experimental animal model which would simulate the clinical revision hip scenario, (2) to determine the effects of alendronate-immobilized calcium phosphate coating on porous tantalum on gap filling and bone ingrowth in a rabbit model, and (3) to develop techniques of improving the bone/implant fixation of porous tantalum joint replacements.

CHAPTER 2: LITERATURE REVIEW

2.1 Introduction to artificial hip joints

Since the 1960s, when the artificial hip joint with polymer liner was developed and applied by John Charnley [12], many improvements have been made, and the total hip replacement (THR) has become an industry worth billions of dollars. Nowadays, many different materials such as cobalt-chromium alloys, titanium alloys and tantalum are being used to ensure the biocompatibility of THR, and different rough surface treatments such as beads and meshes are employed to enhance bone attachment to THR implants. The biocompatibility here is defined as "the ability of a synthetic or natural material for medical implantation to receive the appropriate reaction from recipient environment" [13].

An artificial hip joint typically includes an acetabular shell for attaching to the pelvis, a polyethylene liner for reducing friction and an artificial femoral head and stem for inserting into the femoral intramedullary canal. One example of these hip joint replacements is a titanium alloy stem with dents of 2 to 3 millimeters and an acetabular shell with porous titanium alloy fiber mesh on top(Fig. 2.1).

Recently, porous tantalum, also known as trabecular metal, was adopted for manufacturing the acetabular shell (see Fig. 2.2) [14]. This sponge-like porous tantalum had 400 to 500 micrometer pores that allow bone to grow into them. The outcome of this implant design was the mechanical interlock of the pelvis bone with the acetabular shell, resulting in improved bone / implant fixation.

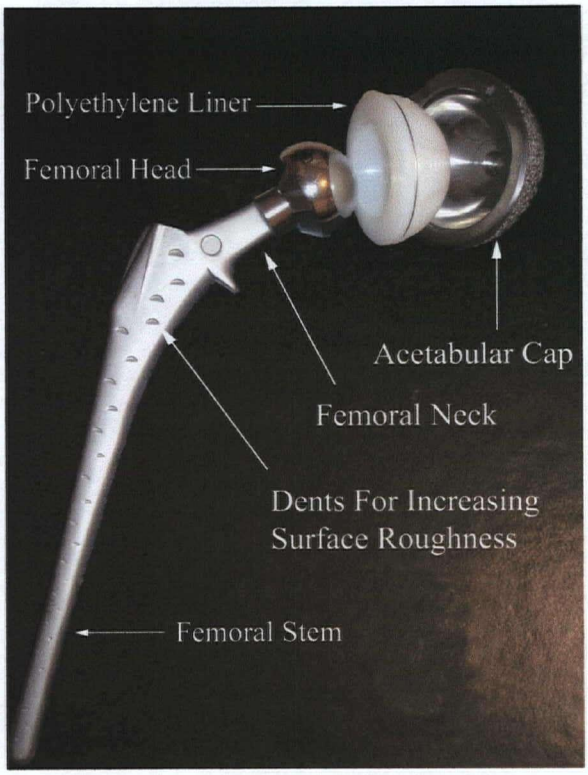

Fig. 2.1 The illustration of an artificial hip joint

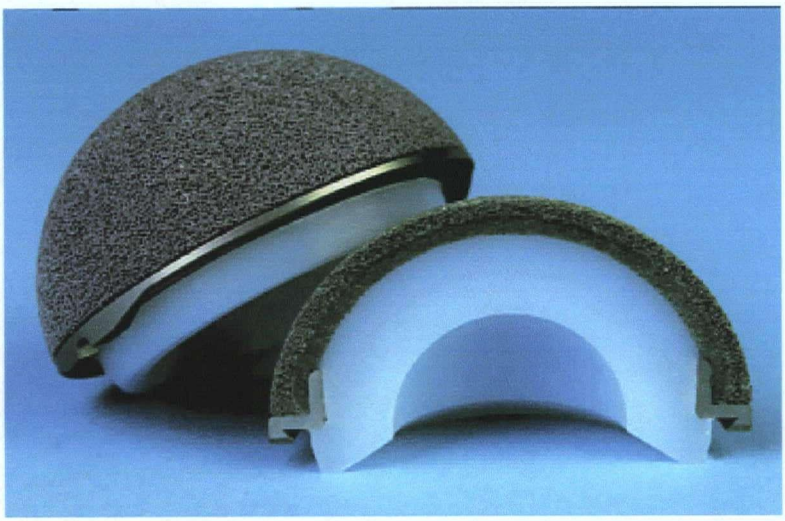

Fig. 2.2 The acetabular shell made of porous tantalum (reprinted from ref. 14, with permission from J of Bone and Joint Surg.)

2.2 Bone

Knowledge of bone, such as its physical and chemical properties, structures, and reactions to wounds etc., is essential to developing joint replacements. Bone is the main *in vivo* environment that joint replacements deal with, and bone is also the target that implants should imitate. Also, bone will undergo a healing process due to the interference caused by implantation. A brief review is provided to illustrate the structure, mechanical properties, and the formation and healing process of bone.

2.2.1 Structure of bone

The structural components of bones are calcium minerals, collagen proteins, water, and some non-collagen proteins. The two main components of bone are minerals and collagen proteins, which contribute to more than 90 % of its weight [15,16]. The bone minerals are primarily carbonated apatite plates with dimensions of up to 50 nm by 25 nm by 3 nm. The collagen proteins are mainly type I and fibrous, and assembled from triple-helical collagen molecules that are 300 nm in length by 1.2 nm in diameter (see Fig 2.3 Level 1 and Fig 2.4 Sub-nanostructure). The mineral plates and collagen fibers assemble together to form the mineralized collagen fibrils [17].

The mineralized collagen fibrils are the building blocks of bones (see Fig 2.3 Level 2 and Fig 2.4 Sub-nanostructure). These mineralized fibrils are 50-100 nm in diameter and up to a few millimeters in length. Bundles of collagen fibrils form individual sheets, or bone lamellae, which stack together to make the lamellar structure [16].

The Haversian system, or the secondary osteon (Fig 2.3 Level 5 and Fig 2.4 Microstructrure), is a small unit of bone with central blood canals (Haversian canals, about 50 μm in size) surrounded by bone lamellae. When bone becomes old or fractured, bone cells start the remodeling process [18, 19]. Osteoclasts resorb the bone and generate the tunnels. Following osteoclasts, osteoblasts rebuild the bone layer by layer as lamellar bones. The central tunnel also functions as a blood vessel with smaller channels of canaliculi connected to it. The canaliculi also connect to osteocytes and supply them with nutrition.

At the macroscale level (Fig 2.3 Level 6 and Fig 2.4 Macrostructure), there are two types of bones classified on the basis of porosity and unit microstructure. Cortical bone, also known as compact bone, is much denser with a porosity of 5 and 10%. It consists of Haversian systems and has fewer blood vessels and bone cells inside it. Also, cortical bone has higher mechanical properties (Young's modulus: less than 30GPa). In comparison, spongy bone, also known as 'cancellous bone' or 'trabecular bone', has a porosity of 50% to 90%. Trabecular bone has much more blood vessels and bone cells, but its mechanical properties such as strength and modulus are lower (Young's modulus of architectural trabecular bone: 0.8GPa).

The pelvis bone is mainly made of the trabecular bone. For a long bone such as a femur, the shaft is mainly made of cortical bone surrounding the marrow. Trabecular bone is found at the two ends (distal and proximal) of the femur next to the joints. The pelvis and the femur are the places where THRs are located.

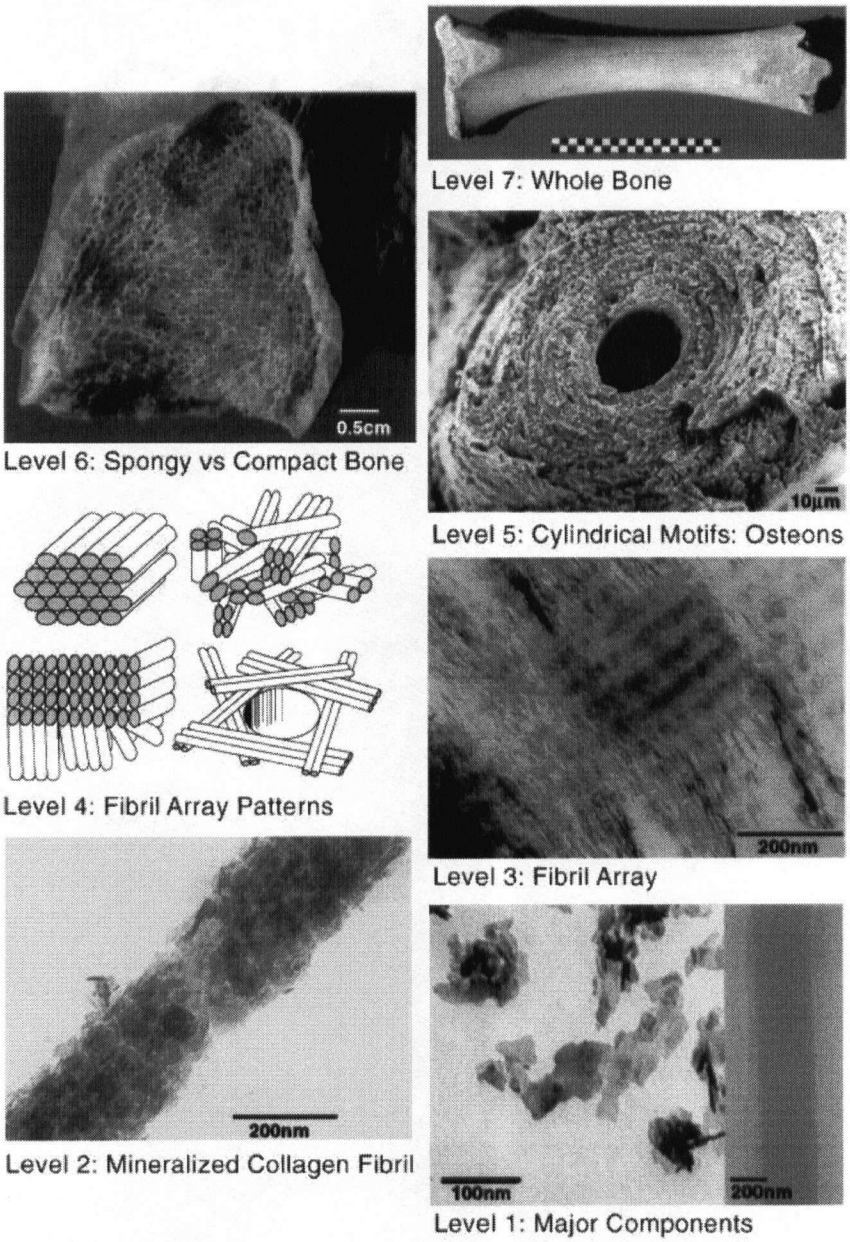

Fig. 2.3 The 7 hierarchical levels of organization of the bone family of materials. Level 1: Isolated crystals from human bone (*left side*) and part of an unmineralized and unstained collagen fibril from turkey tendon observed in vitreous ice in the TEM(*right side*). Level 2: TEM micrograph of a mineralized collagen fibril from turkey tendon. Level 3: TEM micrograph of a thin section of mineralized turkey tendon. Level 4: Four fibril array patterns of organization found in the bone family of materials. Level 5: SEM micrograph of a single osteon from human bone. Level 6: Light micrograph of a fractured section through a fossilized (about 5500 years old) human femur. Level 7: Whole bovine bone (scale: 10 cm). (reprint from ref 16 with permission from Annual Review of Materials Science)

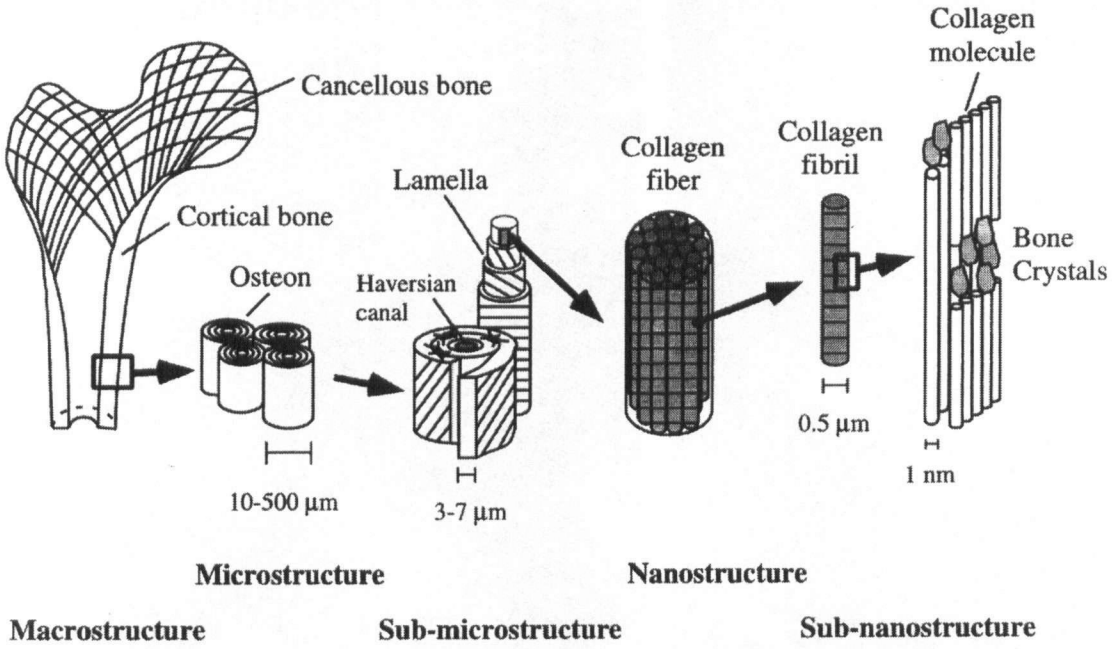

Fig. 2.4 Hierarchical structural organization of bone: (a) cortical and cancellous bone; (b) osteons with Haversian systems; (c) lamellae; (d) collagen fiber assemblies of collagen fibrils; (e) bone mineral crystals, collagen molecules, and non-collagenous proteins. (reprinted from ref 17 with permission from Elsevier)

2.2.3 The mechanical properties of bone

The mechanical properties [20] of lamellar bone are anisotropic. Along the long bone axis the mechanical properties such as strength and modulus etc. are higher than those transverse to long bong axis. With the tested angles varying from 0 to 90 degree, the mechanical properties reduce by 3 to 5 times. For example, the bending strengths reduce from 350MPa or higher at 0 degree to 100MPa at 90 degree; flexural modulus decrease from 16GPa to 7GPa; and the work of fracture (the energy to break the material) reduces from 8kJ/m^2 to less than 1kJ/m^2 [21]. The reason for these differences is because of the fibril structure inside lamellar bone, in which collagen fibrils are parallel to the long bone axis. Also, the body weight applies loadings on the long bone axis, and so they are expected to be stronger in that direction.

2.2.4 Bone formation and bone healing process

Bone healing is a complex biological process [22]. It needs the coordinated actions of growth factors, osteoclasts, osteoblasts and immune cells, etc. within the bone marrow. Stem cells that are recruited from the surrounding tissues and the circulation will differentiate into osteogenic cells. Multiple factors control these chains of reactions and further affect the different sites in the osteoblast lineage through various processes such as migration, proliferation, differentiation, inhibition, and protein synthesis.

Cortical bone and trabecular bone experience different healing processes [23]. Trabecular healing depends on osteoconduction and *de novo* bone formation. On the other hand, cortical healing relies on the remodeling of bone osteons.

The *de novo* bone formation can be divided into four-steps [24]. First, differentiating osteogenic cells, which are the cells still possessing traveling capacity but will become osteoblasts, produce collagen-free organic matrix that provides nucleation sites for calcium phosphate mineralization. Then, calcium phosphate nucleation happens on the collagen-free organic matrix, and the initiation of collagen fiber assembly follows as the third step. Finally, calcification of the collagen compartment will occur.

Cortical healing process can be divided into five major periods including inflammatory, granulation tissue formation, callus formation, lamellar bone deposition and remodeling [25]. And osteoclasts involve in bone healing at two different periods. The population and activation of osteoclasts are extremely high at the early stage of bone healing

because the major function of osteoclasts is to resorb bones. They clean up the broken bone and supply minerals and proteins for the formation of new bones.

The second period we see the high activation of osteoclasts is in the bone remodeling process [25]. The newly formed bone during fracture healing is woven bone, which does not have the regular bone structure. The woven bone can be regenerated fast and bear certain loads. This helps to quicken the healing of injuries. The woven bone will be remodeled later to the regular structure with osteons, canaliculi and nerves, etc. At the remodeling stage, osteoclasts resorb the woven bone and create tunnels, and then the osteoblasts regenerate the lamellar bone surrounding those tunnels. The combination of osteoclasts and osteoblasts activities generates osteons and completes the bone healing process.

Contact osteogenesis and distance osteogenesis [23, 26] are the criteria used to determine whether implant surfaces are osteoconductive (defined on page 12). Contact osteogenesis means that the bone formation happens on the surface of or around the implants, and distance osteogenesis is when the bone starts growing at the site of host bone. If the implant surfaces are osteoconductive, they should induce the bone formation towards them, and both contact and distance osteogenesis will occur. Otherwise, the contact osteogenesis will not happen, and only distance osteogenesis will take place.

2.3 Implant materials

Material selection is very important in artificial joint replacements. The physical and chemical properties of the chosen materials have to fit in the applied physiological

environment and meet the mechanical requirements. Corrosion of implants in an *in vivo* environment is a great concern [27]. On the another hand, the implanted materials must establish a firm interface with the adjacent tissues such as bone, and satisfy the loading needs of natural bone.

The materials suitable for artificial joints include several metals or metal alloys such as stainless steels, titanium, titanium alloys, cobalt-chromium alloy, and tantalum. As these metals or alloys are chosen mainly to fit the biomechanical requirements, the interaction with biological environment is compromised. These metallic implants are usually bioinert and have very limited interactions with surrounding bone tissues. Achieving a strong implant/bone interface has been a challenge [28, 29].

Concepts such as osteoconductivity and osteoinductivity need to be clarified. Both osteoconductivity and osteoinductivity are indicators of the capabilities of bone formation onto bone grafts and implants. Osteoconductivity [30] defines the ability which the graft (porous implant as well) supports the attachment of new osteoblasts and osteoprogenitor cells. It provides an interconnected structure through which new cells can migrate and new vessels can form. Osteoconductivity is the ability of bone graft (or porous implant) to enable new bone to grow through it. Osteoinductivity [30] refers to the ability of a graft (or porous implant) to induce non-differentiated stem cells or osteoprogenitor cells to differentiate into osteoblasts.

Tantalum is one of the metallic materials that have excellent corrosion resistance [31]. It hardly stimulates adverse biological response. Many studies have demonstrated the excellent biocompatibility of tantalum as in bone implants [31, 32, 33]. Solid tantalum may not be good for bone implants because of its high density (16.7 grams/cm^3). The implants made of solid tantalum are much heavier than bone they replace and bring much higher loads to the bone skeleton. The high modulus (200GPa) of solid Tantalum (in comparison to modulus of cortical bone: less than 30GPa) may also cause a 'stress shielding' problem (see page 15).

Porous Tantalum is an ideal implant material that combines its excellent biocompatibility with its mechanical properties similar to those of bone. The clinically available porous tantalum has 75% to 80% porosity, and its elastic modulus is 3 GPa [34]. "The compressive and shear strengths of this porous tantalum are 35 to 40 MPa." [31, 34] Another advantage of porous tantalum is that bone can grow into porous tantalum and construct an interlock system between bone and porous tantalum implants, and the interlock between bone and implant resulted in better bone/implant fixation [34, 35].

The manufacture of porous tantalum is done through a chemical vapor deposition process. Obtaining the desired porosity in the carbon skeleton is achieved through pyrolysis of polyurethane sponge. The tantalum is deposited on the carbon skeleton by chemical vapor deposition with a tantalum pentachloride precursor [34].

2.4 The challenges in hip replacement

Poor implant/bone fixation and an unacceptably high revision rate are the major problems with current joint replacements [4, 5]. Aseptic loosening [36], which is caused by periprosthetic bone resorption (also called osteolysis) triggered by the polyethylene wearing debris entering the joint space [37], is one of the main causes of the implant failure. Another reason is 'stress shielding' which is caused by the metallic materials used for femoral stems.

The present implantation technology is adequate for pain relieving and movement restoring to the ailing hip joints, and the hospitalization time is usually 6 days and full recovery takes about 4 to 6 months [38]. However, many challenges remain unsolved. As the lifespans of human beings continue to increase in the 21st century, the number of patients who need THR will also increase because of the bone problems such as osteoporosis and osteoarthrisis. In 2001, the waiting time for THR surgery in Canada was from 6 to 23 months depending on which province patients lived in [39]. Patients have to endure the serious pain or sit in wheelchairs waiting for their arthroplastic surgeries.

At the same time, the designed implants should extend their longevity to meet the requirement of long post-surgery living time. The existing hip replacements normally can serve patients up to 15-20 years and 20 percents of these hip replacements fail within 20 years. This may cause serious pain to the patients, and new revision surgeries will be needed.

The biological processes of periprosthetic bone resporption (leading to aseptic loosening) include phagocytosis on the wear particles by macrophages, ingestion of debris

particulates and eventually the bone resorption [37, 40]. When wear particles are present, the instinctive reaction (called phagocytosis) of the immune system is to deploy the macrophages to consume these alien particles. Then, the ingestion of particulates of debris starts, and the cytokines and other mediators of inflammation are released simultaneously. These factors then lead cytokines, and other biological components, to activate osteoclasts to resorb bone around the bone/implant interface. Other than polyethylene particulates, metal particles and bone cement particulates also contribute to osteolysis in the same way. The wear debris associate with periprosthetic osteolysis poses a long-term threat to implant longevity [41].

Stress shielding [42] is associated with the load sensing capability of bone and poses a challenge to hip replacements. The lower limbs sustain the load from the body weight and the muscles attached to the long bones exert stresses on the skeleton. Bone is a 'smart material' in that it grows more bone for supporting where the load on bone is larger. For the same reason, it will grow less bone where the load on bone is smaller. The femoral stem of a hip implant (for example, the Young's modulus of Ti alloy is 115GPa) is much stiffer than the cortical bone (Young's modulus is less than 30 GPa) and will take the greater part of the load due to body weight. As a consequence, the femoral bone around the stem is "unloaded", and the femoral bone at the tip of femoral stem is heavily loaded. The loading changes by introducing joint implants to the skeleton induce bone density changes throughout the femur. The upper part of the femoral bone will contain less bone tissue and become more susceptible to fracture. The bone at the tip of implant stem becomes thicker and stronger. Unfortunately, the thickening of the skeleton is often painful [43]. The patients with

cementless stems of total hip devices often feel pain in the thigh, especially during the first year after the surgery.

A major challenge in revision hip arthroplasty is achieving early and durable implant-host bone fixation, especially in the presence of significant bone stock deficiencies. Traditional uncemented implants (porous –coated and titanium fiber mesh) have shown good results clinically in the revision setting. However in cases where less than 50% host bone contact is made the results of these uncemented implants has been less predictable [44].

The message from orthopaedists is that these bone deficiencies, bone/implant gaps and defects are inevitable during the arthoplastic surgeries. Autopsy studies have demonstrated that bone ingrowth occurs in only 30-40% of the surface area of the implant in primary total hip arthroplasty [31, 45]. In revision arthroplasties, bone defects and gaps may significantly compromise the quantity and quality of host bone available for ingrowth. In many cases less than 50% of the host bone is available for ingrowth of the newly implanted shell. To any porous implant material, the reliable and durable bone ingrowth with limited host bone contact is considered a desirable improvement. The improvement would result in an implant that is more versatile in the challenges of revision cases.

2.5 Current material approaches to improve implant-bone fixation

To achieve early implant-bone fixation, many new approaches have been launched to enhance the bone growth on the metal implant surface. Hydroxyapatite, bone morphogenic proteins (BMP) and other materials are introduced either for their similarities of crystal

structure to bone minerals or for their biological functionalities in the bone formation processes.

Sumner et al [46, 47] have studied the effects of BMP on post-surgical bone formation in a canine model. They dipped the implants into different types of BMPs, such as rhBMP-2, before the implant surgeries and examined the bone growth 4 weeks after surgery. The results were positive on enhancements of BMPs on bone formation. Recently, they conducted new animal tests of a gap model with combined addition of BMP-2 and the transforming growth factor β 2 (rhTGF-β2) on hydroxyapatite-plasma-sprayed titanium implants [48]. Compared with non-treated control samples, significant increases in bone formation towards implants were reported on BMPs treated implants. The downsides of BMP treated implants are their low efficiency due to the quick liberation of BMP, the unexpected calcification of surrounding soft tissue, the challenges of obtaining growth factors, storage and transportation, and their low versatility.

2.6 Calcium phosphate

There are several forms [49] of calcium phosphate. Dicalcium phosphate dihydrate (DCPD; $CaHPO_4 \cdot 2H_2O$), tricalcium phosphate (TCP; $Ca_3(PO_4)_2$), octacalcium phosphate (OCP; $Ca_8H_2(PO_4)_6 \cdot 5H_2O$) and hydroxyapatite (HA; $Ca_{10}(PO_4)_6(OH)_2$) are commonly used for implants or implant coatings. The solubility of these calcium phosphates in a physiological condition is generally in following order from highest to lowest: DCPD>OCP>TCP>HA. The pH of the solution also affected the solubility of these calcium

phosphates. In general, as the pH increases from 3 to 9, the solubility of all four forms of calcium phosphates decreases [50, 51].

Because of the similarity of hydroxyapatite to bone mineral contents, hydroxyapatite has been studied as an implant material for many years. The crystal structure of hydroxyapatite is hexagonal with a=9.4 Å and c=6.9 Å cell dimensions [52]. As a type of ceramic, hydroxyapatite is considered brittle. Its fracture toughness (K_{IC}) is less than 0.9 $MPa \cdot m^{1/2}$, and compressive and tensile strengths are less than 300 MPa and 50 MPa respectively. Based on its low mechanical properties, hydroxyapatite alone can not be the load bearing prosthetic material for bone. It is often used as a coating on metallic implants.

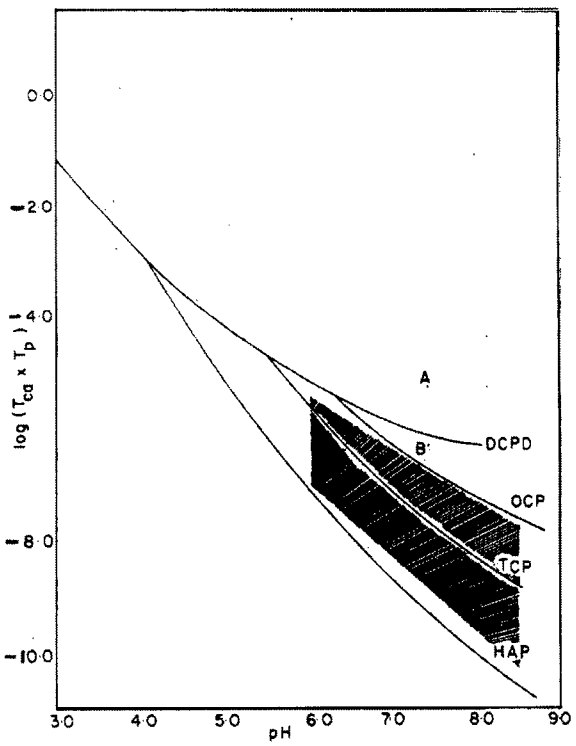

Fig. 2.5 Logarithm of the product of calcium and phosphate concentrations plotted against pH values of solutions saturated with respect to various calcium phosphate phases in the ternary system $Ca(OH)_2$-H_3PO_4-H_2O Calculated for 37°C.(reprinted from ref 50 with permission from American Chemistry Society Publications).

Phosphate conjugates into several forms such as PO_4^{3-}, HPO_4^{2-} and $H_2PO_4^-$. In diluted aqueous solution, the existences of phosphate forms depend on the pH of solution. When the solution is strongly basic (high pH), the phosphate mainly exists as phosphate ions (PO_4^{3-}); when the solution is mildly basic, the phosphate is mostly hydrogen phosphate ions (HPO_4^{2-}); when the solution is mildly acidic, the phosphate is comprised of dihydrogen phosphate ions ($H_2PO_4^-$). This knowledge is essential for the deposition of calcium phosphates from an aqueous solution.

2.7 Deposition of hydroxyapatite

There are many methods for depositing hydoxyapatite on metal surfaces. These methods include plasma spray, biomimetic deposition, sol-gel deposition and electrolytic deposition and so on. Electrolytic deposition (ELD), which is also called electro chemical deposition (ECD), is one of the non line-of-sight coating methods that are suitable for depositing hydroxyapatite on complex 3-D surfaces. Therefore, ELD is the ideal method for depositing hydroxyapatite on porous tantalum.

Plasma spray deposition of hydroxyapatite[53] is the most popular method for orthopaedic implants. The hydroxyapatite powder is heated to a very high temperature (30,000K [54]) by plasma and sprayed on implant substrates. The coatings are lamellar structure [55]. Also, the melted hydroxyapatite may change to other forms of calcium phosphates such as tricalcium phosphate or even amorphous calcium phosphate [55]. There is hardly any chemical bonding between the substrate and hydroxyapatite coating. Thermal stresses are introduced to coatings and to the coating/substrate interface by the high

temperature used in heating. Plasma spray is a line-of-sight process which is not suitable for complex 3D structures such as porous tantalum because only the superficial pores can be coated.

Biomimetic coating of calcium phosphate [56] is a process that mimics the natural mineralization mechanisms in bone. During the coating process, substrates are simply immersed in a supersaturated calcification solution and the coatings grow onto substrates in matter of hours to days. Biomimetic coating of calcium phosphate is attractive because the obtained crystals bear more similarities to the composition of bone minerals, its morphology and structure, and the heat treatment of coating can be eliminated. Also, this method is non line-of-sight and is suitable for complex structures. Cui et al [56] coated porous tantalum using the biomimetic method and obtained a flower-like calcium phosphate coating of calcium phosphate (see Fig.2.2).

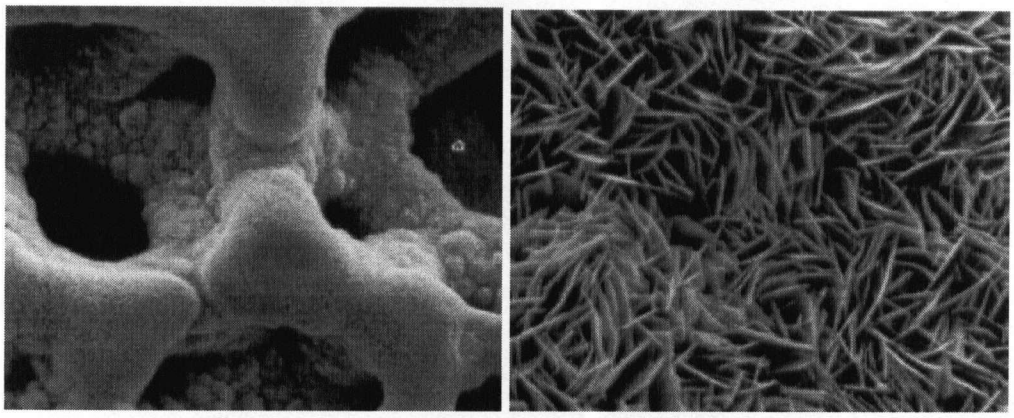

Fig. 2.6 SEM images of biomimetic coatings of CaP on porous tantalum (reprinted from ref. 56, with permission from Springer).

The downside of the biomimetic method is the requirement of a strict chemical environment and surface treatment. For the HA crystals to nucleate, the surfaces of prosthetic

metals need to be chemically etched (e.g. acid/alkaline treatment) or functionalized with negatively charged groups such as sulfonate [57], carboxyl and phosphate [58]. On the native Ti surface without chemical modification, as crystallization theory predicts, the synthesizing parameters need to be strictly controlled [59].

Electrolytic deposition of calcium phosphate is another non line-of-sight process. It takes advantage of the electrode reactions in aqueous solution, and deposits the calcium phosphates on the cathode. When the electrical field is applied, the following cathode reactions will happen [60]:

$$2H^+ + 2e \rightarrow H_2\uparrow$$

$$2H_2O + 2e \rightarrow 2OH^- + H_2\uparrow$$

$$O_2\,(aq) + 2H_2O + 4e \rightarrow 4\,OH^-$$

These reactions will raise the pH of the solution surrounding the cathode. As mentioned above, the solubility of calcium phosphates (DCPD, OCP, TCP and HA) drops while the pH of the solution increases (see page 17 and 18). By controlling the pH of electrolyte and the concentrations of calcium and phosphate ions, different forms of calcium phosphates may deposit on the cathode where the prosthetic metal substrates locate.

Our group [61] has developed an ELD coating technique that can achieve porous structural coatings of hydroxyapatite on titanium and tantalum. The porous structures of hydroxyapatite with pore size of 1 micrometer provide surfaces for bisphosphonate immobilization. The combination of the ELD coatings of hydroxyapatite and the

immobilization of bisphosphonates is one of the promising surface treatments for porous tantalum orthopaedic implants.

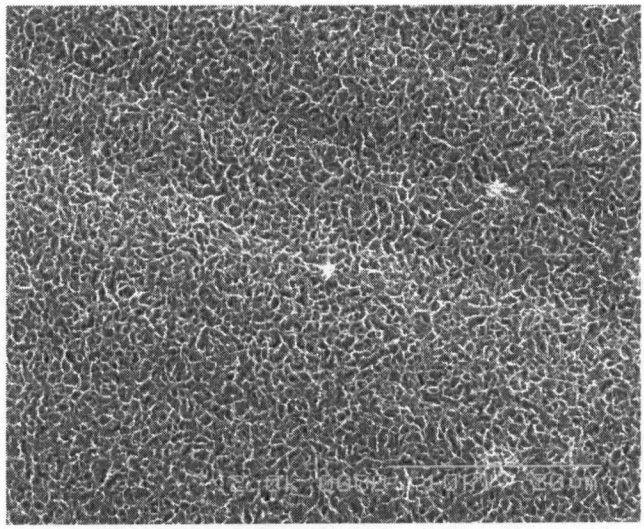

Fig. 2.7 SEM image of the ELD coating of calcium phosphate.

2.7 Effect of bisphosphonates on bone

Bisphosphonates are a family of drugs that have been clinically used to treat osteoporosis and to prevent bone fracture [62, 63]. The effects of bisphosphonates on bone are the decrease in the activities of osteoclasts and the increase of the activities of osteoblasts. Both osteoclasts and osteoblasts, which resorb bone or deposit minerals on tissue respectively, are bone-related cells. The two effects of bisphosphonates mentioned above, are the enhancement of bone formation and an accelerated healing process after arthroplasty surgery [64,65]. Fig.2.8 is the molecular structure of alendronate which is one of the bisphosphonate families.

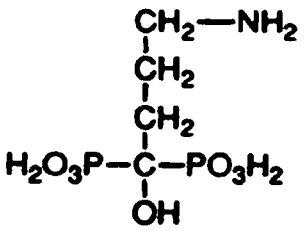

Fig. 2.8 Chemical structure of alendronate (reprinted from ref. 66, with permission from The American Society for Pharmacology and Experimental Therapeutics)

Another chemical characteristic of bisphosphonates is their affinity with calcium ions. Bisphosphonates can chelate with calcium and form bisphosphonate and calcium bonds [59]. This characteristic enables bisphosphonates to be immobilized on hydoxyapatite and create an *in vivo* device that slowly releases bisphosphonates.

2.8 Current studies on bisphosphonate-delivery implants

The effect of zoledronate, which is one type of bisphosphonates, on bone ingrowth into porous tantalum implants was examined in a canine model [67]. Zoledronate in saline was administered in a single post-operative intravenous injection at a dose of 0.1mg/kg. At 6 weeks post-surgery, bone ingrowth increased by 85 % compared with controls. Subsequently, an investigation where zoledronate bound to hydroxyapatite coated (by plasma spray) porous tantalum was performed by the same group [68]. The study demonstrated an increase in peri-implant bone within the intramedullary (inside bone marrow) canal (32.2 % versus 13.8 % in controls) and intra-implant bone formation (19.8 % versus 12.5 %). However, the authors acknowledged the effect of the normal reparative stimulus to reaming the canal, resulting in greater peri-implant than intra-implant bone formation. Also, the plasma spray of

hydroxyapatite is a line-of-sight process in which only the superficial layer of porous tantalum was coated.

Some researchers designed bisphosphonate-delivery methods on different implants materials targeting different implantation locations, and they reported positive effects on enhancing bone growth. Peter et al [69] soaked plasma spray hydroxyapatite coated titanium alloy in zoledronate for THR, and Binderman et al [70] applied alendronate on alveolar surfaces before they implanted the dental replacements.

2.9 Gap model animal tests

Traditional uncemented implants (porous coated and titanium fiber mesh) have shown good results clinically in the revision setting [71]. However in cases where less than 50% host bone contact is made the results of these uncemented implants have been less predictable [44]. Porous tantalum is a relatively new porous biomaterial, which may represent an improvement from conventional uncemented materials. Its properties of a high coefficient of friction (average 0.86±0.11 and 0.98±0.17 against surface-flattened cortical bone and cancellous bone respectively; average 0.58±0.06 when cancellous bone against surface-flattened cortical bone [72]), interconnected pores and high porosity by volume (80%) [31, 45] make it an ideal material in the revision setting with compromised host bone.

The experimental animal tests should replicate the real case scenario during the arthroplastic surgeries. Orthopaedists cannot prepare a patient's pelvis to exactly match the artificial acetabular cup during arthroplastic surgery, especially in the case of bone

deficiencies caused by trauma, bone cancer and former damages revealed in revision. The gaps between bone and the acetabular cup are inevitable. A newly developed implant not only has to enhance the grown bone-implant attachment, but also has to overcome the gaps between host bone and implant.

To simulate the real case, a gap model animal test is necessary. Studies [48,73] showed that gaps of 0.5 to 3 mm inhibited bone ingrowth, and the inhibition increased with the size of the gap. The gap model animal tests should consider the bone size of the tested animal and the implant size to decide upon the proper gap size.

2.10 Mechanism of labeling

The fluorochromes can chelate with the calcium atoms in hydroxyapatite and attach themselves to newly mineralizing front of bone [74]. Only the newly mineralizing surfaces can be labeled probably because of the difference of crystal sizes of hydroxyapatite between initial stages of mineralization and older mineralization sites [75]. The crystal size of hydroxyapatite is smaller at initial stages of mineralization than at older sites.

The commonly used fluorochromes for bone labeling are calcein, alizarin complexone and tetracycline etc. [74]. On retrieved bone samples, these fluorochromes reveal different colors under a fluorescent microscope with the proper light sources and filters. At different postoperative time-points, different fluorochromes can be administrated, and the mineralization process of newly formed bone is completely monitored [76]. However,

the injection dosages have to be carefully controlled because of the potential poisoning of these fluorescent chemicals.

Pautke et al [77] developed a practical labeling protocol on mice bones. They adopted 8 different fluorochromes and sequentially injected them into mice bodies with a 3 day interval. Eventually, they labeled 7 time-points during 4 weeks of bone growth. They claimed that they could observe 6 different fluorescent bands by means of spectral analysis after 6 months, and 4 bands by the naked eye with proper filters.

Frosch et al [78] applied 4 different types of fluorochromes, which are xylenol, calcein, alizarin complexone and tetracycline, to study the enhancement of autologous osteoblast on ingrowth inside drilled 400-600 micrometer holes on titanium substrates. Specimen rabbits were injected with fluorochrome every 5 days postoperatively. The color labeling provided the 'wood pattern' rings of different post surgical time.

2.11. t-tests

Statistics, as a mathematic tool, is often used for medical and clinical studies [79]. Researchers and medical doctors constantly need to draw conclusions on the effects of a pharmaceutical product or a medical procedure based on the symptoms of a small number of patients to those of the whole patient population. Individual patients differ from one another, and so it is essential to use proper methods in evaluating received data. This is the sample representation problem [79]. Another problem is the comparison among the data groups [79]. Based on the measured data, are there any differences among the data groups and are these

differences significant? t-test is one of the statistical methods comparing two groups of data at a time to answer these questions.

There are several different types of t-tests, such as equal size or unequal size, dependent or independent, based on the two groups of data [80]. The t-test is equal or unequal size depending on whether the two compared groups have equal data points or not. The t-test is dependent or independent regarding whether there is any relation between two compared groups or not. If one sample is tested twice or two samples are matched or 'paired', the t-test is dependent; otherwise it is independent.

Before t-test, we assume that the data points follow the 'normal distribution', and the means and the data distribution curves of two compared groups are not different (null hypothesis) [80]. The null hypothesis is either sustained or rejected based on the t-test result and the selective confidence level. The confidence level is the degree of certainty that a statistical prediction is accurate, and it is normally chosen to be 95 or 99%. p-value is "a measure of probability that a difference between groups during an experiment happened by chance.... The lower the p-value, the more likely it is that the difference between groups was caused by treatment."[81] For instance, if the confidence level is chosen to be 95%, p-value, as the result of t-test, has to be bigger than 0.05 (1 minus the confidence level 0.95) to sustain the null hypothesis. Otherwise the null hypothesis is rejected, and the difference between two compared groups is caused by treatment.

t-test starts with the calculations of the arithmetic averages ($\overline{x}$) and the standard deviation (σ) of the data points of the two compared groups ($\overline{x}_1$ and σ_1 for group 1; $\overline{x}_2$ and σ_2 for group 2). N represents the number of data in a group(N_1 for group1 and N_2 for group 2). The degree of freedom is "a measure of the number of independent pieces of information on which the precision of a parameter estimate is based" (courtsey of Wikipedia). For the independent t-test with unequal sizes, the degree of freedom is the number of data minus 1. Therefore the degree of freedom in total is N_1+N_2-2. The t-value can be calculated as following (assume the $\overline{x}_1$ is bigger than $\overline{x}_2$)[82]:

$$t = \frac{\overline{x_1} - \overline{x_2}}{\sigma_d} where \sigma_d = \sqrt{\frac{\sigma_1^2}{N_1} + \frac{\sigma_2^2}{N_2}}$$

Once the t-value is calculated, it can be compared with the tabulated t-value at the degree of freedom and chosen confidence level (tabulated probability p equals 1 minus confidence level) from Student's t table (see Appendix A) [82]. If the calculated t is bigger than the tabulated t, the difference of the two compared groups is significant. In this case, the calculated t can be compared with higher confidence level. Eventually, the p-value can be decided. If the calculate t is smaller than the tabulated t, p-value of t-test is considered bigger than the tabulated probability p, and the difference between the 2 compared groups is not significant.

CHAPTER 3: SCOPE AND OBJECTIVES

The scope of this research is to design a proper gap model of animal tests and to conduct one cycle of animal testing to study the effects of a newly developed alendronate-delivery-coating treatment on the osteoconductivity and bone ingrowth of porous tantalum implants. The experiments include implant processing such as electrolytic deposition of calcium phosphate and alendronate immobilization. Animal tests include surgeries and postoperative animal care, data collection and analysis include histology, histomorphometry and statistic analysis. The project requires collaboration with the Faculty of Pharmaceutical Sciences, the Department of Orthopaedics and the animal centre at the Vancouver General Hospital.

The newly developed coating treatment takes advantage of the effects of alendronate on bone cells to reduce bone resorption and enhance bone formation, and combines with the electrolytic deposition calcium phosphate coating as a delivery vehicle. ELD coating of calcium phosphate is a non line-of-sight process suitable for complex 3D structures such as porous tantalum, and the porous morphology of calcium phosphate coatings provides surfaces for alendronate adsorption. The final product is a combined device of orthopaedic implants with a local alendronate delivery function, which is expected to improve the bone/implant fixation.

The design of animal tests has to simulate the real clinical scenario and to separate the effects of alendronate from any other potential factors. The gap model design is employed

because the bone/implant gaps are inevitable during revision arthroplasty surgeries. The calcium phosphate coatings on porous tantalums are used as second controls. The fluorescence labeling method is employed to track the new bone formation and therefore also allows for studying the mechanism of bone formation.

The objectives of this research are:

1. To modify an existing technique of electrolytic deposition of calcium phosphate to be suitable for porous tantalum substrates.
2. To immobilize an effective amount (dosage of 250×10^{-9} M/L to 10^{-4} M/L per day) of alendronate onto the calcium-phosphate-coated porous tantalum implants.
3. To design a proper gap model of animal tests that can replicate the real case scenario of arthroplasty and revision surgeries.
4. To conduct one cycle of animal tests to evaluate the effects of alendronate delivery coating treatment on osteoconductivity and osteoinductivity of porous tantalum implants.
5. To study the bone formation mechanisms on different surface treatments of porous tantalum implants for the further understanding and improvement of implant surface treatments.

CHAPTER 4: MATERIALS AND METHODS

Bone deficiencies, bone/implant gaps and defects are inevitable during revision arthoplastic surgeries [44]. The experimental designs of animal tests should replicate the clinical scenario. The intention of the gap model animal tests was to investigate the bone reaction towards different surface treatments of implant materials in the presence of a gap between the implant and bone. As a result, the better implant surfaces in terms of overcoming gaps and enhancing bone/implant fixation could be determined.

This animal study of alendronate-immobilized calcium-phosphate-coated porous tantalum implants included implant preparation, sterilization of implants and tools, implant surgeries, post surgery care of animals, sample harvest and sample analysis. The implant preparation included pre-coating surface cleaning, electrolytic deposition of calcium phosphate, alendronate immobilization, cap mold design and bone cement cap manufacture, and cap assembling. The sample harvest and sample analysis step included euthanasia, femur dissecting and sectioning, bone histological processing and embedding, and histology and histomorphometry analysis.

4.1 Implant preparation

4.1.1 Porous tantalum

The porous tantalum implant (Trabecular Metal ™) cylinders, which were 3.18 mm in diameter and 8 mm in length, were provided by Zimmer Inc. (Warsaw, Indiana, USA). The pore sizes of these tantalum plugs were about 400 to 500 micrometers (shown in Fig.

4.1), and the porosity of these porous tantalum was about 75%. The density of solid tantalum was 16.65 g/cm^3. Weighted with a 1/100,000 g balance (Mettler AE240), the weights of five porous tantalum implants were listed in Table 4.1, and the average weight was 0.237 (SD 0.014) g.

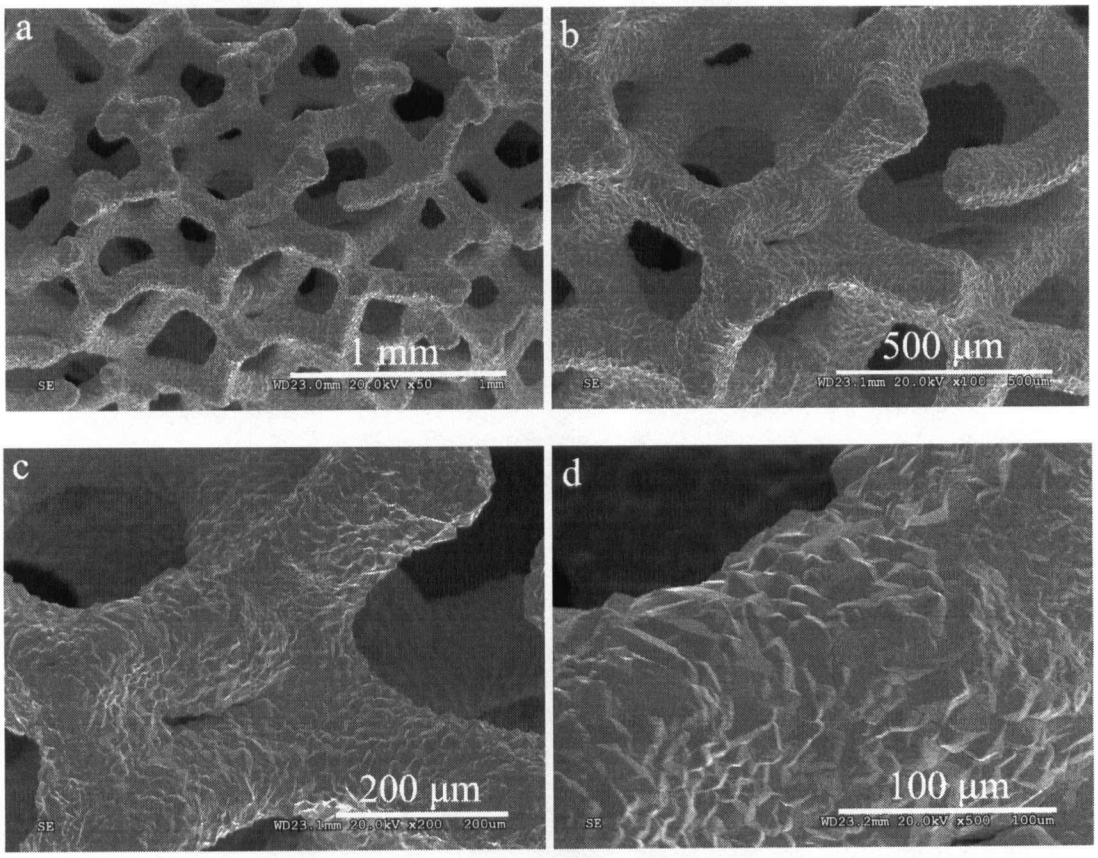

Fig. 4.1 SEM images of porous tantalum cylinder at various magnifications.

Table 4.1 The weight of porous tantalum implant plugs

No.	1	2	3	4	5	average
Weight (g)	0.225	0.237	0.261	0.228	0.235	0.237 (SD 0.014)

The surface area is a parameter, which affects current density, for porous tantalum plugs as substrates for electrolytic coating of calcium phosphate. The estimation of surface

area was based on the assumption that the porous tantalum plug was built with a single tantalum tube wrapped in cylindrical space of the 3.18mm in diameter and 8mm in length. The dimensions of this tube are 0.15 mm for outer diameter and 0.03 mm for inner diameter, as measured on BSE images. Based on the average weight and the density of tantalum we could calculate the volume of solid tantalum, which was then converted to the tube surface area. The surface area of an implant plug thus estimated as 395 (SD 23.7) mm^2.

4.1.2 Electrolytic deposition (ELD) of calcium phosphate coatings

4.1.2.1 Surface cleaning of tantalum specimens

Surface contamination such as grease and non-uniform oxidation of metal substrates etc could affect coating kinetics, uniformity and morphology. Specimens needed to be cleaned properly before coating. The porous tantalum cylinders were ultrasonically bathed in acetone for 3 minutes and immersed in high concentration sulfuric acid (95 wt% H_2SO_4) (Fisher Science Inc) for 1 minute. The high concentration sulfuric acid can dehydrate and destroy the organic molecules. Both steps were designed to eliminate any organic contamination. The porous tantalum cylinders were then rinsed and cleaned in ultrasonic bath of distilled water for 3 minutes, and then rinsed 5 times in distilled water to remove sulfuric acid (20ml or more water for more than 5 min each time).

The residue of sulfuric acid from surface cleaning process should not effect bone cell reaction to implants. In animal or human bodies, there are about 0.3 mM/L sulphate in their serum [83], and these sulphate anions come from food, water and air. After rinsing, the

residue of sulphate anions from implants should be much less than the sulphate anions in blood stream. "Excess sulphate in the blood is rapidly eliminated by urinary excretion" [84].

4.1.2.2 ELD coating cell fixture

A customized electrolytic cell fixture for electrolytic deposition was designed and manufactured in biomaterial laboratory (shown in Fig 4.2). The fixed interval between 2 electrodes, which were cathode for implant plugs and anode for 25×25mm platinum plate respectively, is 9 mm. It was measured from the surface of the platinum plate to the closer parallel tangent surface of the porous tantalum cylinder. The anode clip was made of stainless steel which was not immersed in the coating electrolyte, and the cathode rod which fully contacted with the porous tantalum cylinder was made of tantalum. The porous tantalum cylinders were completely immersed in the electrolyte during ELD deposition.

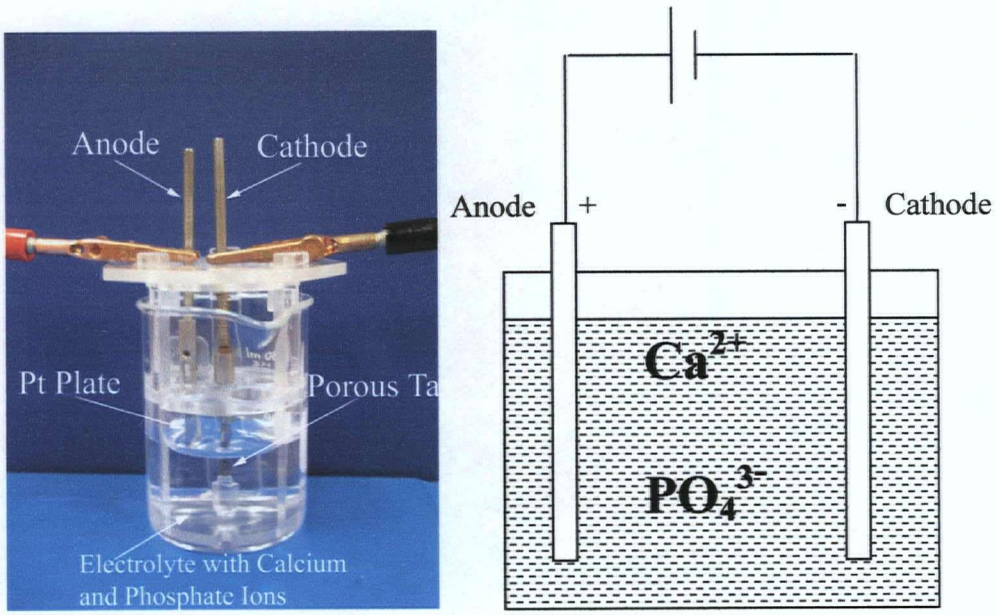

Fig. 4.2 The image and schematic illustration of ELD coating cell

4.1.2.3 ELD coating parameters

In order to study calcium phosphate coating parameters, the crystal structure of the coating, and the morphology and thickness of calcium phosphate coatings, 100-micrometer thick tantalum foils of 20×20mm and porous tantalum blocks of 3×3×8mm were used. Only half of the square tantalum foil was immersed in electrolytic solution, therefore the surface area of this electrode was 400mm^2 which was close to the surface area of porous tantalum cylinders. The dimensions of porous tantalum blocks were chosen to have a closer geometric shape to the porous tantalum cylinders.

The modification of coating parameters was conducted based on the ELD coating technique developed by our group [61]. The parameters were selected to avoid the formation of hydrogen bubbles which harms the adhesion of coatings, and the formation of DCPDs which affects the uniformity of coating structure and morphology. Other criteria, such as the cracking of coatings, the thickness of coatings and the uniformity of thicknesses of coatings at both inner and outer pores, which is particularly important for porous tantalum, are evaluated as well. The goal is to achieve coatings that are crack-free and have homogeneous micro-porous structure with a uniform thickness of 3 to 5 micrometers of calcium phosphate throughout the porous tantalum cylinder.

Some of the coating parameters, such as the concentrations of calcium and phosphate ions in the coating electrolyte, pH of the solution and the applied voltage, and so on, have already been optimized [61] and were used without being changed in this study. Periodical stirring was introduced to increase the thickness uniformity across at central pores. The effect

of periodical stirring is examined by comparing coatings with and without this process. Coating time was chosen to achieve the maximum thickness of coatings with minimum cracking. The modified processes of ELD of calcium phosphate are as follows.

The ELD of calcium phosphate was carried out in an aqueous solution that contained calcium and phosphate ions which was prepared by adding proper amount of calcium nitrate ($Ca(NO_3)_2 \cdot 4H_2O$), ammonium dihydrogen phosphate ($NH_4H_2PO_4$) and sodium chloride (NaCl) (Fisher Scientific). The concentrations of calcium and phosphate ions were 5.25 mM and 10.5 mM respectively, and the concentration of Sodium chloride was 150 mM. The pH of the solution was then adjusted to 5.25±.07 by adding 1N sodium hydroxide (NaOH) under the monitoring of a calibrated pH meter (Thermo Orion, Beverly, MA. USA). The applied DC voltage was 2.6 V, and the duration of coating was 3 hrs. During the coating period, the coating solution was periodically stirred every 30 minute which should enhance the ion supply to the centre pores of implant plugs.

4.1.3 Alendronate immobilization

Bisphosphonates contain two phosphonate groups attached to a single carbon atom (C), forming a P-C-P structure. Alendronate (monosodium 4-amino-1-hydroxybutylidene-1,1-diphosphonate trihydrate) was the bisphosphonate used in the study. It was chosen because of its efficacy, availability, and clinical record.

The immobilization of alendronate (Sigma Aldrich) was carried out by immersing calcium phosphate coated implants in 3.2 ml 10^{-4} M sodium alendronate in 0.01 M Phosphate

Buffer Saline (PBS) solutions at 37°C for 7 days. Proportion of besphosphate ions from solution were adsorbed by the calcium ions on the Ca-P coating surfaces. Then, the soaked implants were rinsed with distilled water five times (20ml or more water for more than 20 min each time). The rinsing steps ensured that most of the non-adsorbed alendronate ions were removed from implants.

4.1.4 Implant assemblies

The gap model was achieved by installing polymethymethacrylate (PMMA) bone cement (Simplex ® P, Stryker Howmedica Osteonics, Limerick, Ireland) caps at both ends of the implant plugs. The caps act as spacers between bone and the porous tantalum plugs. As a result, the desired gap between the implant and the surrounding trabecular bone was maintained when the caps were press-fitted to the pre-drilled holes in the femoral bone. The final gap is a 0.6mm thick cylindrical wall with the inner diameter of 3.18mm and an outer diameter of 4.37mm. The volume of the gap zone is about 35 mm^3. The details of the dimensions of the final implant assemblies are illustrated in Fig. 4.3. Bone cement was used as the material for caps because it is clinically used in orthopaedic surgeries. Also, the flexible mixing ratio and adjustable curing time make it an ideal casting material.

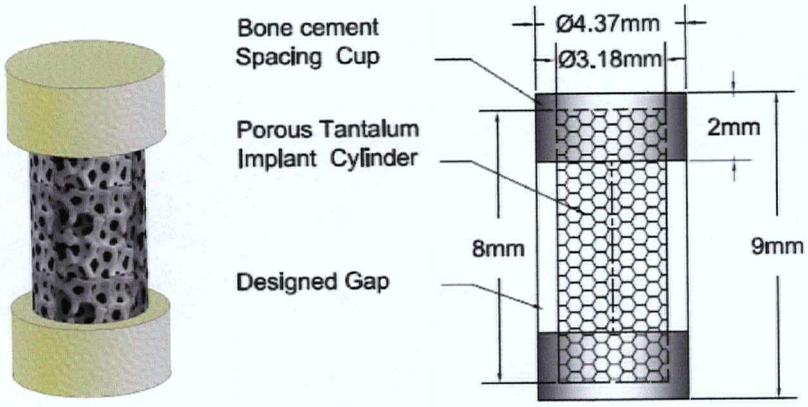

Fig. 4.3 Mechanical drawings of porous tantalum implant assembly. The left is a 3D drawing of the implant assembly, and the right is a 2-D drawing with all the dimensions

Four customer-designed molds (Fig.4.4) were machined and used to cast bone cement caps. The ratio for bone cement was 0.7 grams of powder per 0.5ml of monomer liquid, which allows 5 min of viscous state for handling. The dimensions of the cap were 4.37mm in outer diameter, 3.18 mm in inner diameter, 2mm in height and 1.5mm in depth. During assembly, the implant plugs were carefully handled to avoid any damage to the coating surfaces, and a drop of bone cement (same ratio as above) was added into each cap as a glue to firmly attach the 2 caps to each end of the implant cylinder (Fig. 4.3).

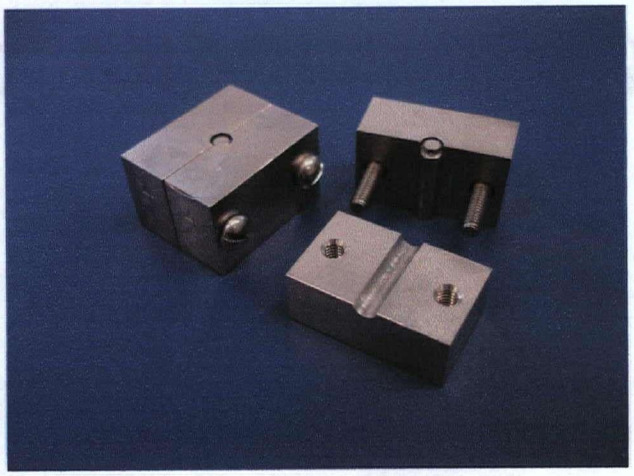

Fig. 4.4 The image of bone cement casting mold

4.1.5 Sterilization of implants and surgical tools

To minimize any damage to the rabbit's femoral bone, such as cracking during surgical drilling, a set of twist drill bits of serial diametric sizes was employed. They were 5/64" (1.98mm) brad tip, 1/8" (3.18mm) and 11/64" (4.37mm). These drill bits (Lee Valley Co. Canada) were ultrasonically cleaned in acetone and ethanol to remove organic contaminations. Then they were immersed in 70% isopropyl for pre-sterilization before being sealed in polyethylene bags (Food Saver). The implant assemblies were re-sealed in polymer packaging bags from Zimmer (see Fig. 4.5).

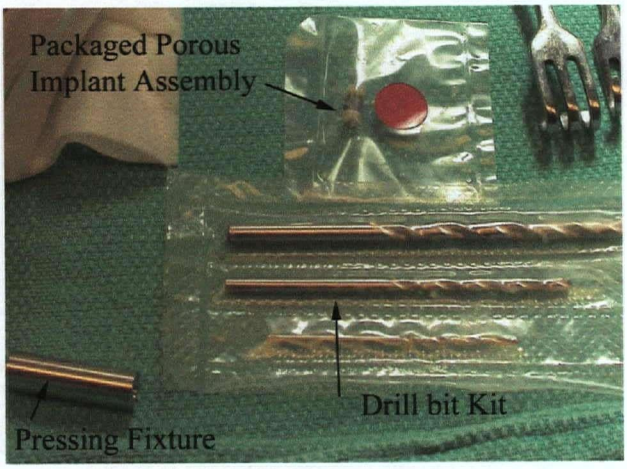

Fig. 4.5 Surgical tools and porous tantalum implant

Beta-ray radiation sterilization was carried out at Iotron Tech. Inc., Canada following the ISO13485:2003 international standard for medical devices. The applied radiation dosage was 25 to 27 KGys. Other tools such as the hand drill and surgical forceps were sterilized by autoclave at Jack Bell centre, Vancouver General Hospital.

4.2 High performance liquid chromatography (HPLC) tests for drug loading

Five alendronate-immobilized calcium-phosphate-coated porous tantalum implants were tested for total amounts of drug loading. They were processed in the same way as the implants for animal tests. These 5 pilot samples were immersed in 1ml 1M hydrochloric acid, and the alendronate-containing calcium salt on the samples was dissolved in the acid solution. The tantalum samples were examined with the Nikon Eclipse optical microscope and the coating was confirmed to be completely dissolved. Seven alendronate solutions with known concentrations, which were 100, 50, 25, 12.5, 6.3, 3.1 and 1.6 μg /ml respectively, were also prepared as standard samples. These samples generated a linear calibration equation between alendronate concentration and a peak area of alendronate ($R^2 = 0.9998$).

During HPLC (high performance liquid chromatography) analysis, solutions reacted with 5 fold (V:V) of 2 mg/ml fluorescamine in acetonitrile to form a conjugate. The acetronitrile was extracted off with dichlormethane. The aqueous phase containing the conjugate was analyzed with a Waters chromatography station, with Nova Pac C18 column and 470 scanning fluorescence detector. The conjugate was detected by excitation at 395 nm and emission at 480 nm.

4.3 Animal tests

Alendronate-immobilized and calcium-phosphate-coated porous tantalum implants were tested in comparison with uncoated porous tantalum as control samples. To confirm the

effects of alendronate on bone formation, calcium-phosphate-coated porous tantalum was adopted as another set of control samples as well. The detailed plan is shown in Table 4.2.

Eighteen New Zealand White female rabbits of 3.5-5.0 kg (28 to 34 weeks old) were employed for the animal tests. They were randomly divided into 3 groups for the 3 types of implant assemblies which are non-treated porous tantalum (Ta) from Zimmer as control samples (6 rabbits), calcium-phosphate-coated porous tantalum (Ta-CaP) as second type of control samples (6rabbits), and alendronate-immobilized calcium-phosphate-coated porous tantalum (Ta-CaP-ALN) (6 rabbits). The animal tests were conducted at the Jack Bell centre (animal centre), Vancouver General Hospital. The study was approved by the Animal Research Ethics Review Board at the University of British Columbia (Protocol number: A04-0275).

Table 4.2 Animal test plan for bisphosphonate-coated porous Ta bone implants

	Ta (Porous Ta control)	**Ta-CaP** (Porous Ta with calcium Phosphate coating)	**Ta-CaP-ALN** (Ta-CaP soaked in alendronate)
Rabbits	6	6	6
Number of implants	12	12	12
Fluorescence labeled samples	12	12	12
Histological sections	36	36	36
SEM/ fluorescene microscopy	36	36	36
Image analysis	36	36	36

4.3.1 Implantation procedures

The implantation location of the distal femur was selected because the trabecular bone inside the femoral distal end is similar to the bone at the pelvis. The rabbit was shaved and then anaesthetized by intramuscular injection of a sleeping dose of 3.15 to 3.5 mg ketamine/xylazine. The anaesthesia was maintained by inhalation of 2% to 2.5% isoflurane. Then, pain killer (0.3mg Buprenorphine, Temgesic) was administrated subcutaneously. The skin of the rabbit, where the incision would take place, was cleaned with 0.5% chlorhexadine and then sprayed with 0.5% dexidin. These pre-surgery procedures were conducted by the animal care staff at the Jack Bell Center.

The surgical procedure on the rabbits was performed by Dr. Winston Kim (a surgeon) in the animal operating room. A 3cm incision was made on the distal lateral aspect of the femur, and the vastus lateralis was split along its fibers to expose the underlying bone. One 4.37 mm hole was made bilaterally through sequential drilling (1.95 mm, 3.18 mm and 4.37 mm) under saline irrigation. The orientation of the hole was perpendicular to the distal femoral condyle, and the depth was confirmed with a depth gauge. The porous implant with PMMA bone cement caps was gently inserted into the hole (see Fig 4.6). The wound was then irrigated and closed in a uniform manner. Two implant plugs with the same surface were implanted in each rabbit, to avoid the confounding influence of the presence or absence of different implant coatings. The anaesthetic, operative procedure and animal care were performed in compliance with University and federal guidelines.

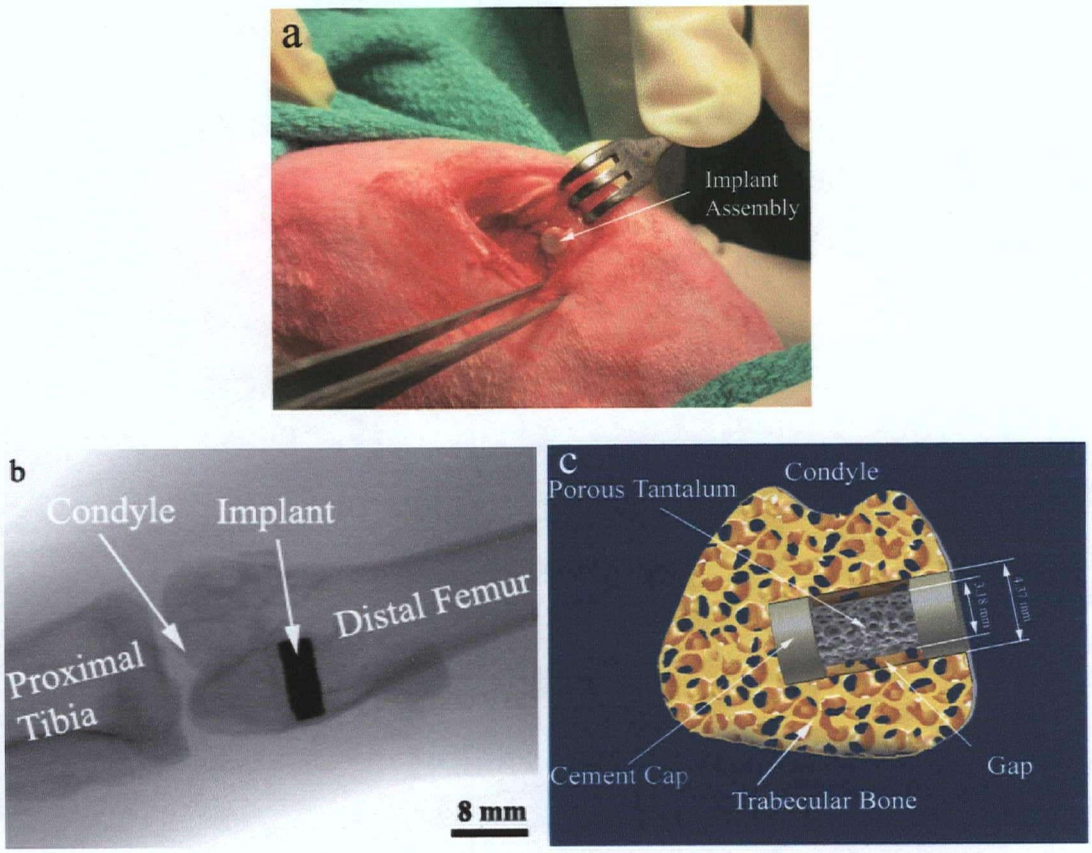

Fig. 4.6 The images and schematic illustration of the implant location. a) digital image of implant position during surgery; b) X-ray image shows the implant position after surgery; c) the schematic illustration

4.3.2 Bone labeling

Bone growth front was labeled with fluorescence dyes to track new bone formation with time. Two commonly used fluorochromes from Sigma-Aldrich, Alizarin complexone (absorption: 530-560 nm, emission: 624-645 nm) and calcein (absorption: 494 nm, emission: 517 nm), are dissolved in distilled water, and sodium bicarbonate was added to reach the concentration of 1.4% wt. The pH of the solutions was adjusted by adding hydrochloric acid if necessary. Within a Type II A bio-safety cabinet, these solutions were filtration sterilized with 0.2 micron filters (Millex GS, Carrigtwohill, Co. Cork, Ireland) and packaged in 10ml sealed syringes. The detail information about these two fluorochromes is listed in Table 4.3.

Table 4.3 Information of fluorochomes and their solutions

	Alizarin compleone	Calcein
Sigma Catalog No.	A3882	C0875
Absorption	530-560 nm	494 nm
Emission	624-645 nm	517 nm
Solution Concentration	30mg/ml	10mg/ml
Solution pH	7.4	7.4

The labeling chemicals were administrated subcutaneously. The labeling should provide information about the direction of bone growth, growth speed and bone growth mechanism. Calcein and Alizarin complexone were chosen because their emission wave lengths are within visual light range which means no special light sources such as ultra violet are needed. Also, these 2 chemicals are relatively mild to rabbits. As shown in Table 4.4, the dosages of calcein and alizarin were 10 and 30milligrams per kilogram of rabbit's body weight respectively.

Table 4.4 Labeling administration dosages and schedule

	Dosage	concentration	Solution volume	Day after surgery
Calcein	10mg /Kg	10mg/ml	1ml/Kg	7^{th} day
Calcein	10mg/Kg	10mg/ml	1ml/Kg	14^{th} day
Alizarin	30mg/Kg	30mg/ml	1ml/Kg	21^{st} day
Alizarin	30mg/Kg	30mg/ml	1ml/Kg	28^{th} day

4.3.3 Animal care after surgery

Antibiotic medicine, Notrile, was administrated after the surgeries. Rabbits were fed with carrots, hay and vitamins, and the weights and body temperature of these rabbit patients were monitored regularly. Force feeding may be applied to those 'depressed' rabbits. Further administration of antibiotics may be applied to those rabbits with higher body temperature.

4.3.4 Euthanasia, radiograph imaging and sample harvest

After 29 days of healing process, the rabbits were intravenously injected with Pentobarbital 2mg/Kg of body weight to stop the heart beat in less than 2 seconds. After the animal deceased, X-ray images were taken to reveal the implant positions. Afterward, the lateral legs were dissected, and then the femoral bones with the implants were removed for further histology analysis.

4.4 Sample analysis

4.4.1 Histology sample preparation

The femur was cut parallel to the radius direction of the condyle arc (see Fig. 4.7). The harvested samples were fixed, dehydrated, infiltrated and then embedded in epoxy resin (SPURR, Canemco, St. Laurent, QC, Canada) following a standard histological procedure (see Table 4.5) [85].

Table 4.5 Processes and schedules for fixation, dehydration and infiltration

Processes	Chemicals	Temperature	Duration
Fixation	10% buffered formalin	20°C	2days
Dehydration	70% Ethanol/Water	20°C	3days
Dehydration	90% Ethanol/Water	20°C	3days
Dehydration	100% Ethanol	20°C	3days
Dehydration	100% Ethanol	20°C	3days
Defat	100% Acetone	20°C	3days
Infiltration	50% SPURR/Acetone	20°C	3days
Infiltration	80% SPURR/Acetone	4°C	3days
Infiltration	100% SPURR	4°C	3days
Infiltration	100% SPURR	4°C	3days

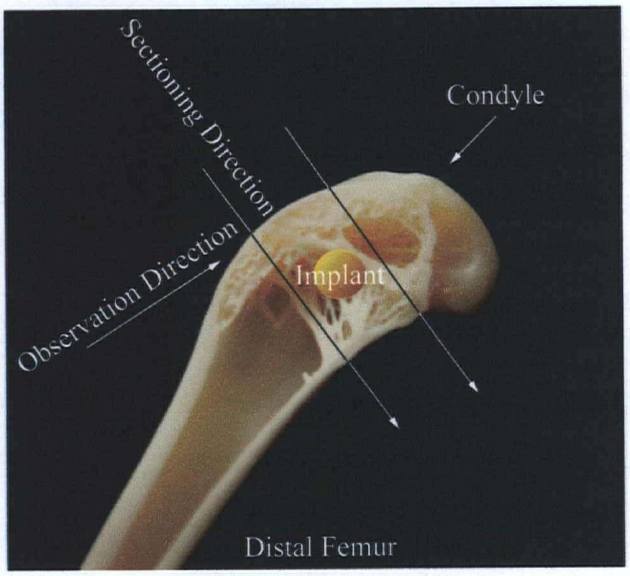

Fig. 4.7 Schematic image for sectioning and observation directions

In order to examine bone formation at the site of the implants and to reveal the 3-D structure, each embedded sample was longitudinally cut with a diamond saw (Buehler, Lake Bluff, IL USA), and ground and polished (Buehler) into three sections at 200 μm, 850 μm and 1500 μm deep from the tangent surface of the implant. Fig.4.8 gives the schematic illustration of the three examining sections.

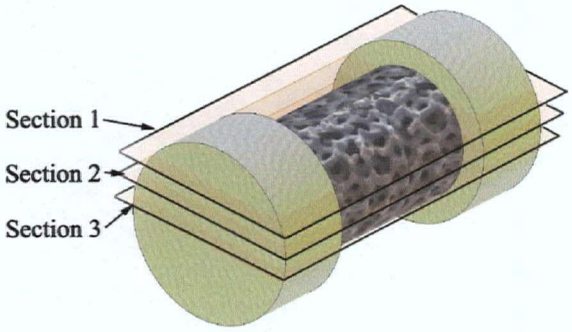

Fig. 4.8 Schematic illustration for three examining sections

After samples were embedded in SPURR (Canemco, St. Laurent, QC, Canada), the examining surfaces were ground to just touch the implant cylinders, which meant the grinding surfaces were the tangent surfaces of the porous Ta implant cylinders. The surfaces were considered the origin of the coordinate. Then the 2 samples from same rabbit were re-embedded together in Epothin (Buehler) resin in a standard (1.25 inch in diameter) mold. After curing, the bottoms of the Epothin blocks were ground parallel to the sample surface with the grinding fixture at an accuracy of ±20μm. The final surfaces were vibration polished with 0.05 micrometer silica slurry.

4.4.2 Histology and histomorphometry analysis

4.4.2.1 Fluorescence microscopy

A fluorescence microscope (Eclipse E 600, Nikon, Tokyo, Japan) with a FITC & TRITC dual exciter and dual emitter filter block, (exciter wavelengths: 475 – 495 nm and 540 – 575 nm, emitter wavelengths 500 – 535 nm and 580 – 620 nm), was used to analyze the fluorescence labels and new bone formation. The fluorescent imaging was performed before sputtering of Au/Pd alloy for SEM. Under the fluorescence microscope, bone formation front in the first 2 weeks was marked by two green calcein labels, while red alizarin Complexone lines marked bone formation in the 3rd and 4th week.

4.4.2.2 BSE imaging

The back scattered electron (BSE) images were taken under a Hitachi-S3000N SEM (Hitachi Scientific Instruments, Tokyo, Japan). Polished samples were sputtered with Au/Pd. BSE mode under high vacuum pressure was used. The beam current was set to 65mA,

voltage was 20 kV, and the aperture was removed. All these setups guarantee bone, epoxy and Ta to have differentiable gray scales which meant the histogram would show 3 peaks.

4.4.2.3 Image analysis

The image analysis was carried out on the low magnification BSE images using image analysis software (Clemex Vision PE 3.5, Longueuil, QC, Canada). The magnification calibration of BSE images with image analysis software was 3.93 μm per pixel. The quadrilateral defined by the 4 corners of caps was considered the sample area. Gray level discrimination was used to identify epoxy, new bone formation and implant. Figure 4.9 shows how Clemex processes the images. Analysis on the 3 sections of BSE micrographs generated quantitative information on total gap volume, total volume available for bone ingrowths, and total volume available for new bone formation.

The volume of bone gap filling, which was new bone formation in the gap region between the tantalum implant and host bone, and bone ingrowth into porous tantalum which was bone formation within the pores of the tantalum plugs, were measured. The total bone formation (the sum of the gap-filling and ingrowth) was then calculated. Total available tantalum length (see Fig. 4.10 (b): black lines) and the contact length (see Fig. 4.10 (a): blue lines) of newly formed bone on the porous tantalum surface of the three longitudinal sections of all implants were also measured. Fig 4.11 gave the schematic illustration of the defined gap-filling and bone ingrowths in this study.

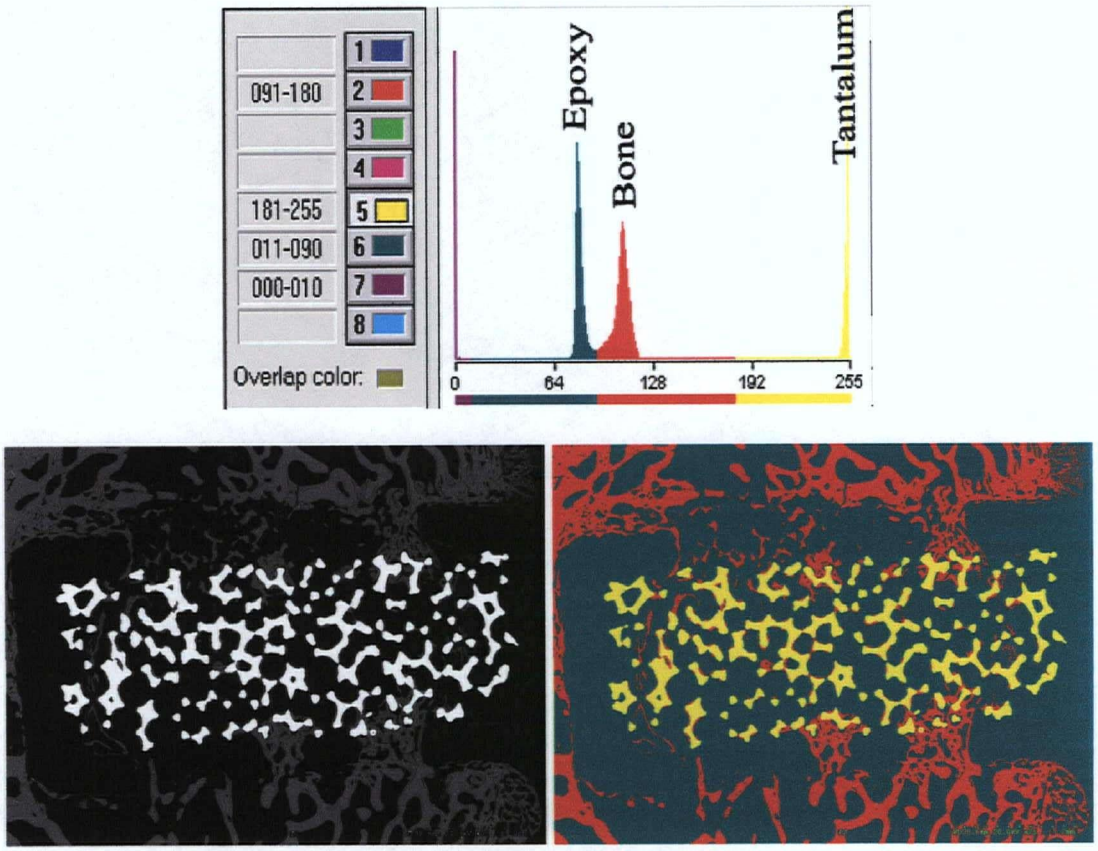

Fig. 4.9 Histogram for image analysis and the images before and after the dying process

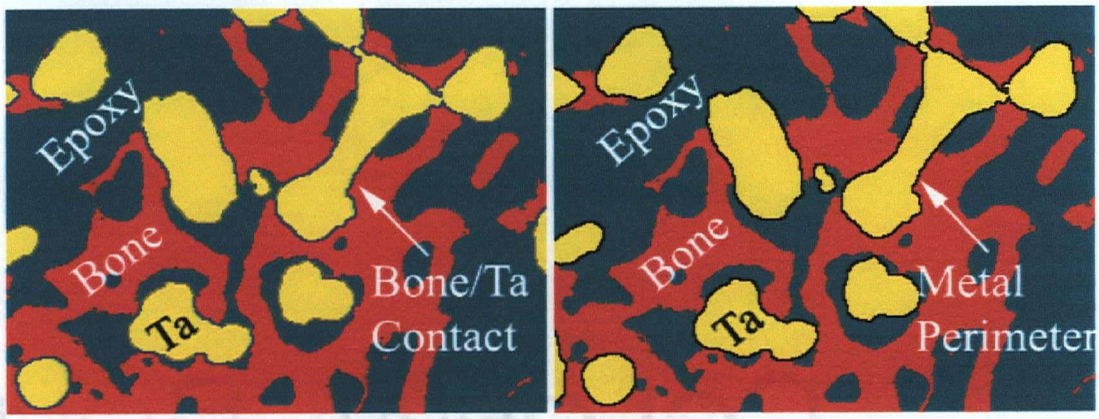

Fig. 4.10 The measuring images for contact length and the available metal length

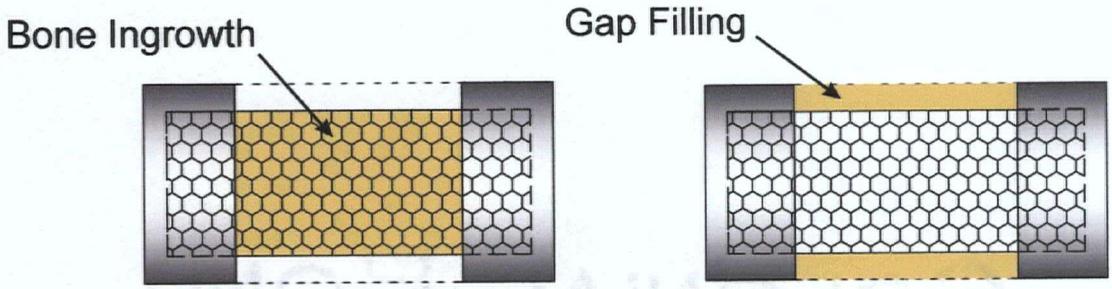

Fig. 4.11 The schematic drawings illustrate the bone ingrowth and gap filling

4.4.2.4 Statistical data analysis

Differences in the mean and standard deviation were investigated by a two-tailed t-test, using a statistical software program (SPSS Version 14.0, Chicago, IL, USA). An independent sample t-test was used to compare the volume of gap filling, bone ingrowth, total bone formation, and the new bone formation contact length of the different implants. We chose 95% for the confidence level and considered a p-value of < 0.05 to be significant.

CHAPTER 5: RESULTS

5.1 The effects of coating parameters on calcium phosphate coating morphology

Many coating parameters such as pH and the temperature of the electrolytes, applied voltage, calcium and phosphate ion concentrations and coating duration affect the final coating crystal structure and coating morphology. Duan [61] has studied these parameters on flat titanium substrates and has optimized the coatings to a micro-porous structure good for drug delivery. To apply this ELD coating technique to porous tantalum substrates for the animal test, the coating process needs to be standardized to achieve repeatable coatings on all the alendronate-immobilized implants and the calcium-phosphate-coated controls. Some coating parameters need to be modified to fit the porous substrates of tantalum.

The porous structure of calcium phosphate coatings can be obtained on porous tantalum substrates by using the same concentrations of calcium and phosphate ions, solution pH and applied voltage as those found on titanium plates. The remaining two major concerns on calcium phosphate coatings were cracking and spallation of coatings and the uneven coating thicknesses at superficial pores and central pores.

Porous tantalum plugs were coated with calcium phosphate without sulfuric acid cleaning. The calcium phosphate did not uniformly cover the tantalum struts. On some samples, uncoated spots surrounded by calcium phosphate coating could be seen (see Fig. 5.1 (a)). With the sulfuric acid cleaning, these phenomena dramatically reduced.

Spallation and cracking of the porous calcium phosphate coating are related to the thickness of the coating if other factors, such as coating porosity, remain constant. Coating duration was chosen to control the coating thickness in our experiments. Observations using an optical microscope were adopted to examine coating surfaces. The duration of the ELD coating process was determined; hence few cracks or crack-free coatings were achieved. Fig. 5.1 (b) shows spallation happening on a porous tantalum sample. The coating duration for porous tantalum implants was shorter than that for this sample.

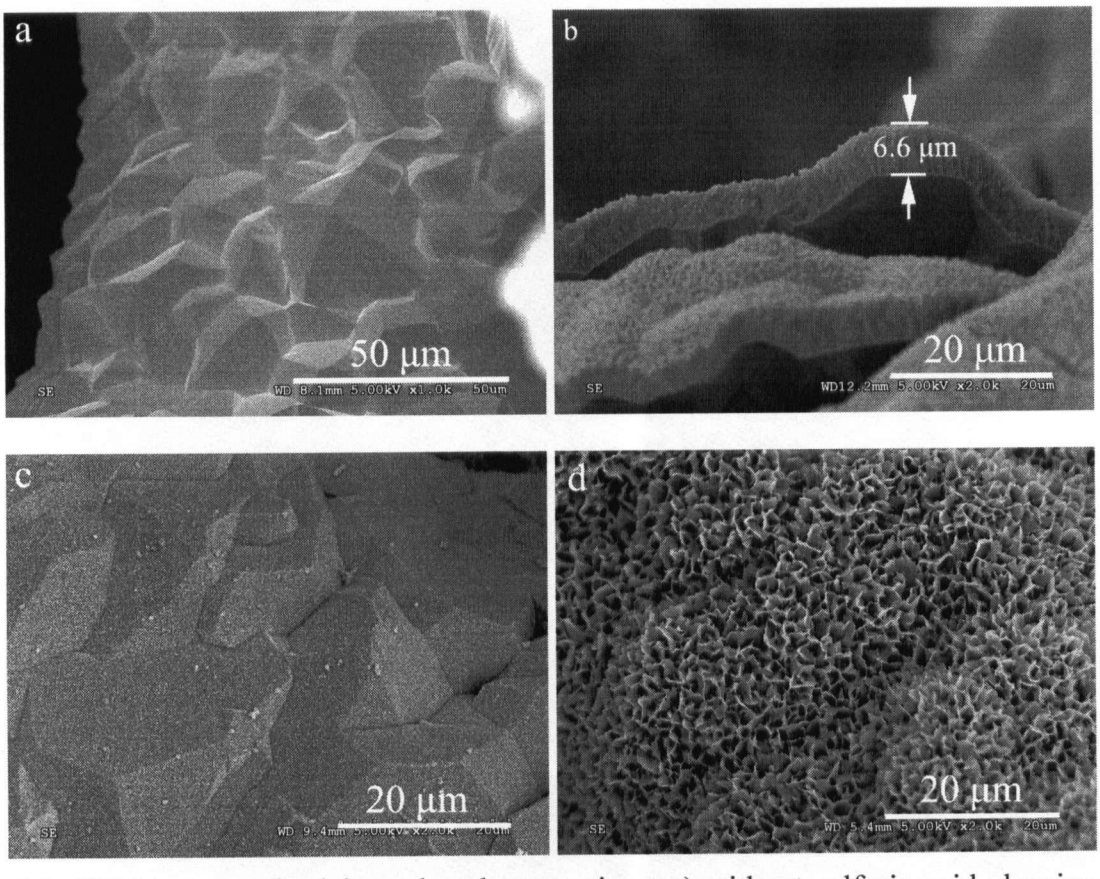

Fig. 5.1 SEM images of calcium phosphate coatings. a) without sulfuric acid cleaning, the porous tantalum strut was not coated; b) spallation of calcium phosphate coatings; c) coatings morphologies at central pores without periodical stirring; (d) coating morphology at superficial layer when periodical stirring was not applied.

Several porous tantalum plugs were coated with calcium phosphate without periodical stirring. Fig. 5.1 (c) and (d) show coatings at the central pores and at the superficial pores on one sample respectively. At the central pores (Fig. 5.1 (c)) the coating was very thin (less than 500 nm), and the sharp edges of the metal grains could be seen. Also, the pore size of calcium phosphate coatings was very small. At the surface (Fig. 5.1 (d)) of the porous tantalum cylinder, larger pores of calcium phosphate coatings were formed, and the metal grain edges were blunt or buried under calcium phosphate coating. The estimated thickness was more than 3 micrometers.

The causes of these uneven coating thicknesses in Figure 5.1 might be the insufficient supplies of calcium and phosphate ions to the central pores because all ion supplies defusing from the surrounding solution were consumed by the superficial layer. Periodical stirring was introduced to the coating process to manually deliver the calcium and phosphate ions into the central pores of porous tantalum as the ion supplies for coating. Fig. 5.2 shows the improved coating at a central pore with the periodical stirring.

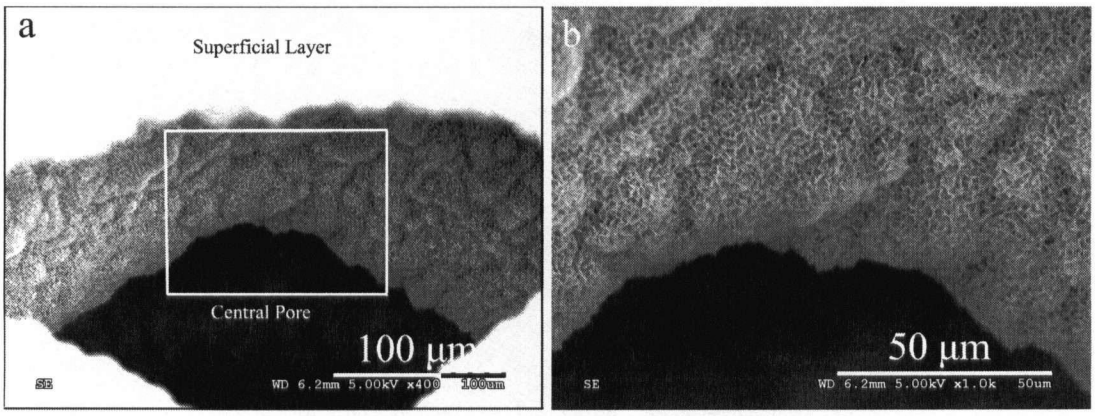

Fig. 5.2 SEM images on calcium phosphate coatings at a central pore when periodical stirring was applied.

5.2 Calcium phosphate coating and alendronate loading

5.2.1 ELD coating of calcium phosphate

The digital image and SEM images under different magnifications (Figure 5.3) show the morphology of calcium phosphate coatings on porous tantalum implants. The digital image (Fig. 5.3(a)) shows the complete implant assembly. The low magnification image (Fig. 5.3(b)) shows that the coverage of the calcium phosphate coating over the complex 3D tantalum structure is almost 100%. Higher magnification images (Fig. 5.3(c), (d)) illustrate the coating morphology which is a thin layer of calcium phosphate with a micro-scale porous structure (about 1 μm in pore size).

A tantalum foil sample was employed to conduct a coating thickness measurement. The coating parameters for this foil substrate were the same as those for porous tantalum cylinders. After coating, the foil was bent 180° to crack the calcium phosphate coatings. The coating thickness was 5.8 micrometers as measured on an SEM image (Fig. 5.4).

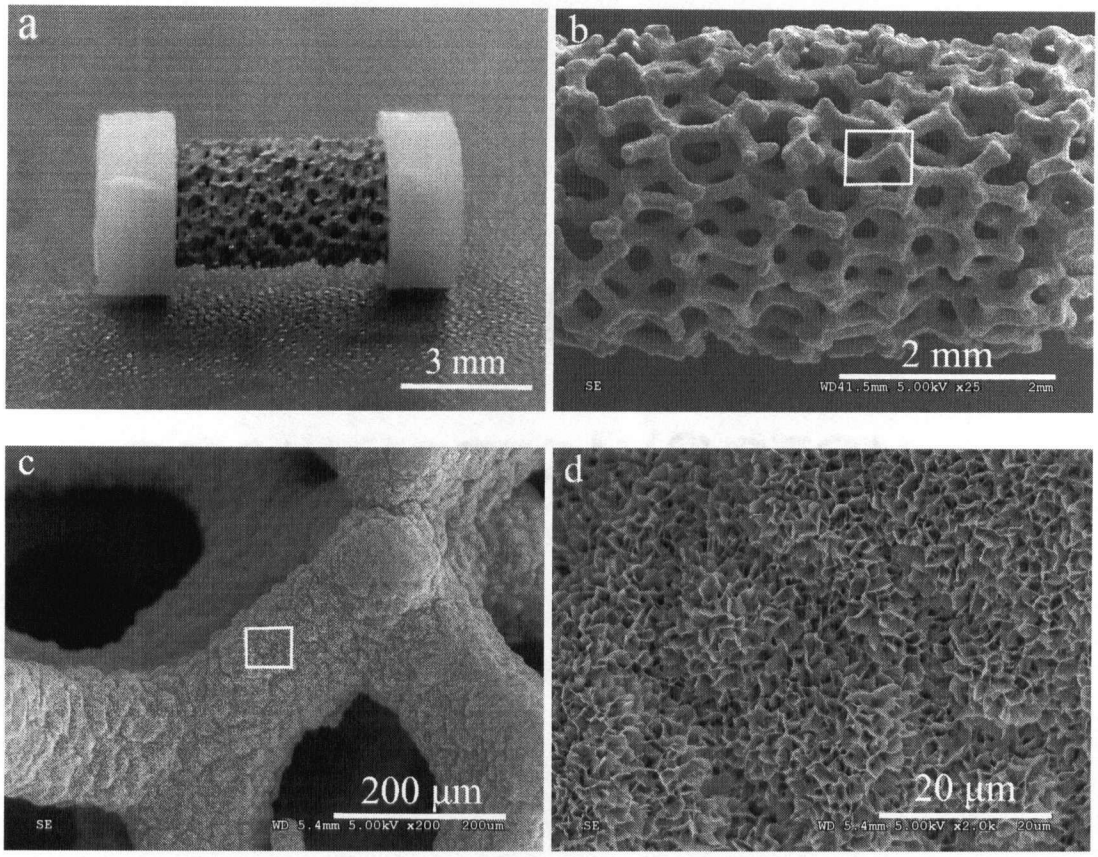

Fig. 5.3 SEM images at varying magnifications of Ca-P coating morphology. a) digital image of implant assembly; b) low magnification SEM image shows the coverage of CaP coating; c) and d) the porous morphology of CaP coating.

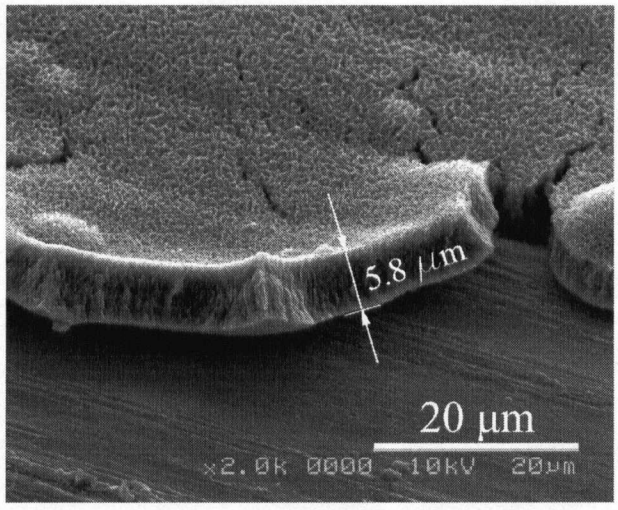

Fig. 5.4 SEM image showing coating thickness

5.2.2 The alendronate loading amount and estimation of dosage

The HPLC experimental results of alendronate loading amount on the 5 pilot porous tantalum plugs were calculated, and the drug dosages were estimated accordingly. The total drug amount loaded by immobilization was at microgram level, and the average drug amount on these 5 porous tantalum plugs was 1.37 (SD 1.0) micrograms. The molecular weight of alendronate was 325.12 grams per mol. The volume of gap was calculated as ~35 mm^3, and the volume of pores was calculated as ~48 mm^3, based on the dimensions and measured porosity of porous tantalum cylinders. The total volume of sample zone was ~83 mm^3.

Assuming that all drugs dissolved in one day, which was the extreme case that was unlikely to happen, the highest possible drug dosage was ~4.7 $\times 10^{-5}$M/L. This dosage was still in the effective zone of alendronate concentrations which were from 250×10^{-9} to 10^{-4} M/L per day according to Bergstrom[86]. In our animal tests, there should not be any concern of overdose of alendronate. If all the drugs and calcium phosphate slowly dissolved in 20 days, the average daily dosage should be ~2×10^{-6} M/L which was within the effective concentration zone.

5.3 Crystal structure of ELD calcium phosphate coating

XRD results showed the ELD coatings to be a mixture of HA and OCP (Fig. 5.5), as evidenced by the diffraction (shoulder) of OCP at $2\theta = 4.72°$ and diffraction of HA at ~50 (49.46 (2 1 3) plane). The standard HA or OCP has higher intensity at 33 degrees than that at 26 degrees. The XRD spectra of ELD coatings (and alendronate-immobilized coatings) have higher intensity at 26 degrees ((002) planes), indicating a preferred orientation of the calcium

phosphate crystals in ELD coatings. Comparing the two XRD spectra, it can be concluded that alendronate immobilization did not change the crystal structure of the calcium phosphate coating.

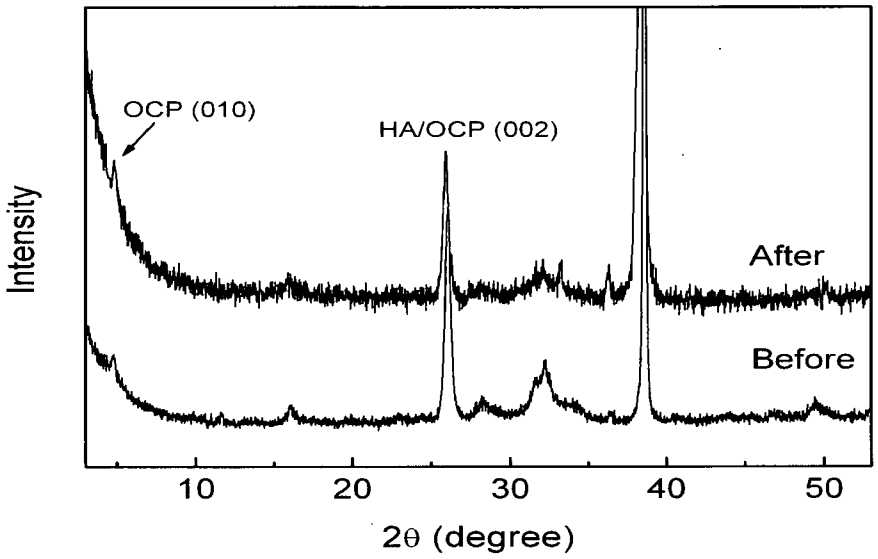

Fig. 5.5 XRD results for CaP coatings before and after alendronate immobilization

FTIR spectra of the coatings before and after alendronate immobilization are shown in Fig.5.6. The PO_4^{3-} peaks at 561 and 600 cm^{-1} are close to those of octacalcium phosphate (OCP), which is one type of calcium phosphate crystal structure with PO_4^{3-} peaks at 561 and 599 cm^{-1}[87]. As a comparison, the PO_4^{3-} peaks of hydroxyapatite (HA) around 600 cm^{-1} are 566.7 and 603 cm^{-1}[88], and the interval between these two peaks is smaller than the current result. After alendronate immobilization, FTIR spectrum shows slight changes at 1080 and ~875 cm^{-1}. FTIR spectrum of alendronate calcium salt shows the P-O stretching modes of phosphonate at 1090, 1000 and 964 cm^{-1} [89]. The changes in FTIR spectrum after

immobilization might be because of the chelation of alendronate and calcium ions on the calcium phosphate coating surfaces.

The energy dispersive X-ray spectrometry (EDS) tests on ELD calcium phosphate coatings were carried out on tantalum foil substrates to compare the coatings of calcium phosphate before and after alendronate immobilization. The atomic ratio of calcium and phosphorus can be used as supporting evidence of the crystal structure because different calcium phosphate crystals have different Ca/P ratio. On each type of coating, five different areas located at the centre and the 4 corners were tested, and the averages of CaP atomic ratios were calculated to be 1.54 and 1.53 before and after alendronate immobilization respectively. The adsorption of alendronate onto the coating thus did not significantly change the Ca/P ratio of the calcium phosphate coating.

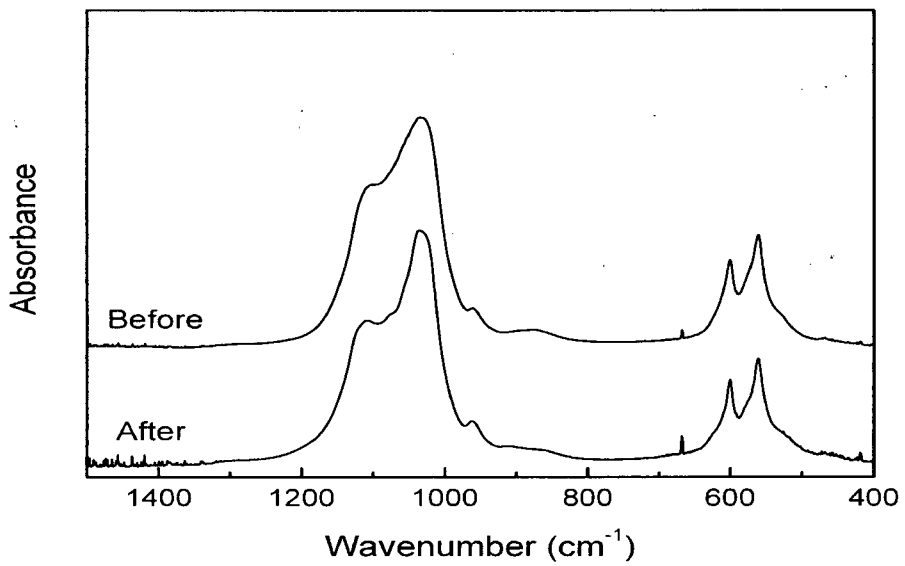

Fig. 5.6 The FTIR results for CaP coatings before and after alendronate immobilization

In conclusion, the crystal structure of the calcium phosphate coatings was not changed during alendronate immobilization based on the results of XRD, FTIR and EDS. The coatings before and after alendronate immobilization are predominantly OCP. However, the existence of HA can not be excluded. The crystals in the ELD coating are oriented.

5.4 Histology

The microscopic analysis of peri-implant bone growth was carried out with a fluorescence optical microscope and a scanning electron microscope. The bone growth patterns, including bone formation, growth directions and the bone/implant interlocking etc, were studied. The comparisons of these histological results between control groups and the drug-loaded group were conducted.

Figure 5.7 shows the BSE images (left column) and fluorescence optical images (right column) of bone growth on the 3 types of implants: Ta control (Fig.5.7 (a), (b)), Ta-CaP control (Fig.5.7 (c), (d)) and Ta-CaP-ALN implant (Fig.5.7 (e), (f)). In the BSE images, it could be obviously seen that peri-implant bone growth and ingrowth into the implant were the highest on the Ta-CaP-ALN sample (Fig.5.7 (e)). Between the 2 types of control samples, the Ta-CaP control had more bone growth in defined sample area than the Ta control did.

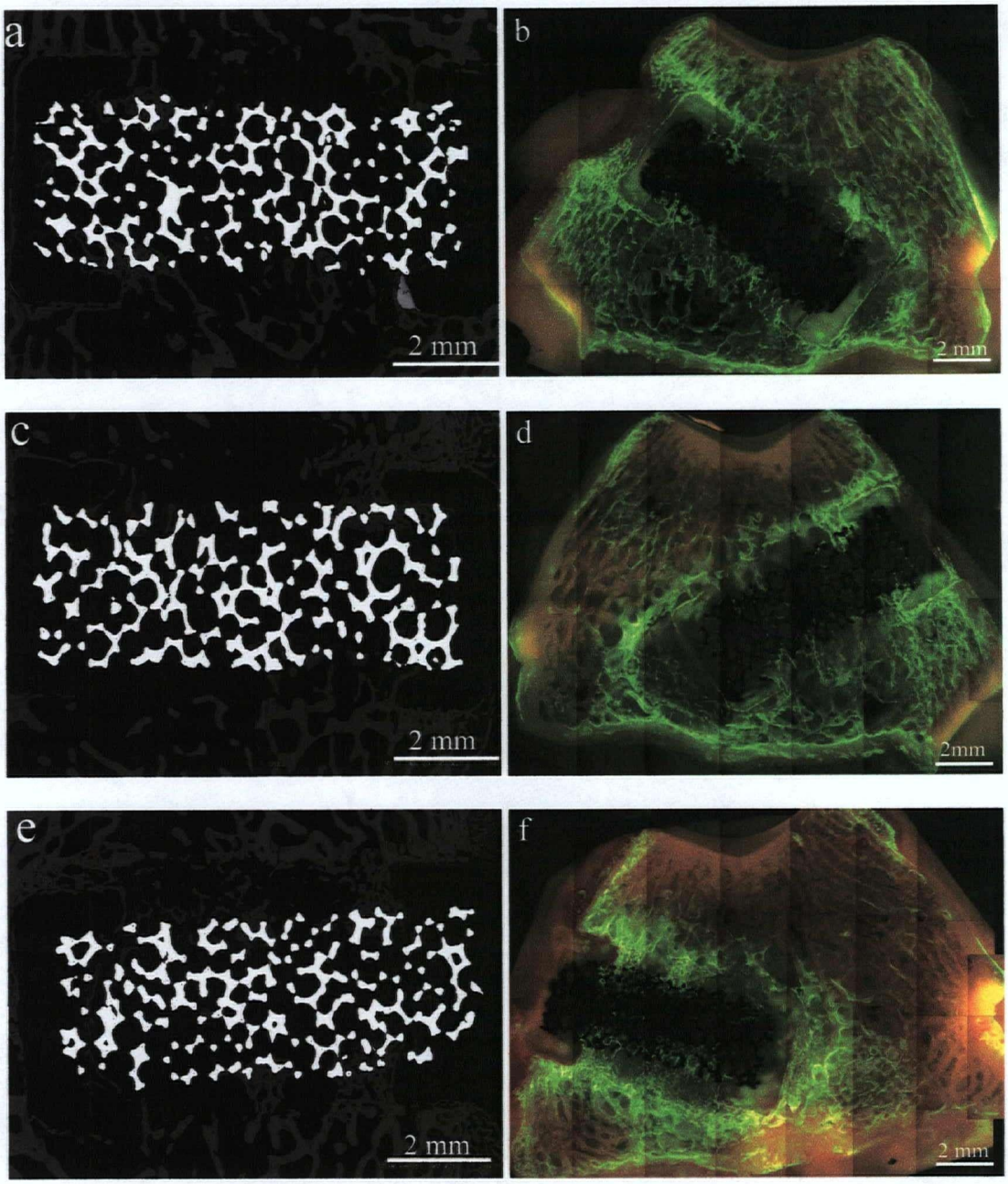

Fig. 5.7 BSE and fluorescence images of bone formations on 3 types of implants. a) and b) non-coated control; c) and d) calcium phosphate coated control; e) and f) alendronate-immobilized calcium-phosphate-coated implant.

The fluorescence optical images in Figure 5.7 show the whole bone sections where the sectioning planes were made along the axis of implant cylinders. The shining green colour was the emission light of calcein under the excitation light of 495 nm wavelength.

Again, we could observe significant increases of bone growth on Ta-CaP-ALN implant comparing with those on the 2 types of controls. Also, the pore size of the newly grown peri-implant bone was smaller in comparison with two other control samples. Furthermore, the green colour indicated that these new bones were formed in the first 2 weeks post-surgery. The depth of ingrowth into porous tantalum implants on Ta-CaP-ALN sample was higher than those on the two types of controls in which ingrown bone only reached the superficial layer of pores.

5.5 Histomorphometry

The ingrowth was the new bone that grew into porous tantalum plugs; the gap filling was the new bone growth in the designed gap area, and the total bone growth was the sum of the ingrowth and the gap filling. The information from 3 sections was integrated into 3-D volume percentages. For the bone/implant contacts, the data were presented separately.

5.5.1 Bone formation

5.5.1.1 Gap filling

The mean extent of gap fillings was 13.0 % (SD 5.0 %) for Ta controls, 15.8 % (SD 3.3 %) for Ta-CaP-ALN controls, and 29.1 % (SD 10.0 %) for Ta-CaP-ALN implants (shown in Fig 5.8). The relative increases in volume of gap fillings on Ta-CaP-ALN implants were 124% (2.24 fold) and 84% (1.84 fold) compared with Ta controls and Ta-CaP controls respectively.

The t-tests, comparing Ta-CaP-ALN implants with Ta controls, indicated the difference of gap fillings between these two groups was significant (p-value was less than 0.0001) (see Table 5.2). Between Ta-CaP-ALN implants and Ta-CaP controls, the difference of gap fillings was significant as well (p-value was less than 0.0005). On the other hand, the calcium phosphate coating slightly increased the bone formation volume of gap filling, but the p-value of t-test was 0.12 which meant that the difference of gap fillings between these two groups were not significant.

5.5.1.2 Bone ingrowth

The mean volume of bone ingrowth was 6.0 % (SD 2.7 %) for Ta controls; 8.3 % (SD 2.9 %) for Ta-CaP controls, and 19.9 % (SD 5.9 %) for the Ta-CaP-ALN (see Fig.5.8). The increases in bone ingrowths on Ta-CaP-ALN samples were 232% (3.32 fold) and 140% (2.40 fold) compared with Ta controls and Ta-CaP samples respectively.

The p-value of the t-test in comparison of Ta-CaP-ALN implants with Ta controls resulted in less than 0.0001 which meant the difference of ingrowths between these two groups was significant (see Table 5.1). The difference of ingrowths was also significant between Ta-CaP-ALN implants and Ta-CaP controls (p-value was less than 0.0001). In comparison to Ta controls, bone ingrowth was slightly increased on Ta-CaP samples, but the p-value of the t-test was 0.07 which meant the increase of bone ingrowth on Ta-CaP samples was not significant.

5.5.1.3 Total bone formation

The volume of total bone formation, which was the sum of gap filling and bone ingrowth, was 9.7 % (SD 3.5 %) for Ta controls, 12.4 % (SD 3.2 %) for Ta-CaP controls and 26.2 % (8.3 %) for Ta-CaP-ALN implants. The increase of total bone formation on Ta-CaP-ALN implants was 170 % (2.7 fold) compared with that on Ta controls. The increase was significant because the p-value of t-test was less than 0.0001. The total bone formation on Ta-CaP-ALN implants showed a 111 % (2.11 fold) increase in comparison to Ta-CaP samples, and it was also statistically significant ($p < 0.0001$).

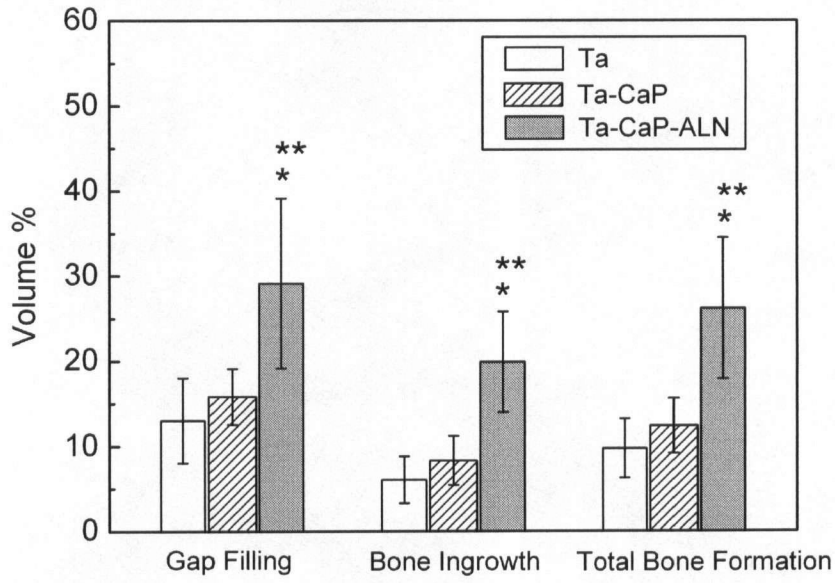

Fig. 5.8 The mean and standard deviation of volume of gap filling, bone ingrowth and total bone formation. Ta-CaP-ALN implants demonstrated significantly increased gap filling, bone ingrowth and total bone formation compared with Ta-CaP controls ($p < 0.0005$, $p < 0.0001$ and $p < 0.0001$ respectively *), and significantly increased gap filling, bone ingrowth and total bone formation compared with Ta control ($p < 0.0001$, $p < 0.0001$ and $p< 0.0001$ respectively **). No significant differences in gap filling, bone ingrowth and total bone formation were found between Ta-CaP and Ta. ($p = 0.12$, $p = 0.07$, and $p = 0.07$).

Table 5.1 The p-values of t-tests on bone formation, gap filling and ingrowth

Compared groups	Bone formation, v%	Gap filling v%	Ingrowth v%
Ta & Ta-CaP	0.07	0.12	0.07
Ta & Ta-CaP-ALN	< 0.0001	< 0.0001	< 0.0001
Ta-CaP & Ta-CaP-ALN	< 0.0001	<0.0005	< 0.0001

5.5.2 Bone/implant contact length

The direct contact between newly grown bone and the implant is a very important factor that affects the mechanical fixation of implants. This is especially critical when there is a gap existing between the implant and its surrounding host bone, the contacts between newly formed bone and the implant directly dictate the implant fixation.

In the 2D sections, the contacts between bone and implant only encounter new growth bone because the gap model design avoids any press-fit contacts of host bone and implants. Also, the bone/implant contact interfaces in 3D structure becomes the border lines between bone phase and implant metal phase in the 2D images. The length of these contact border lines directly represents how well the new bone contacts the implants. Therefore, the bone/implant metal contact length can be used as a criterion to judge the bone/implant contact and the implant fixation.

The mean percentages of bone-implant contact length over total available tantalum length of the three sections were measured (Fig 5.9). In section 1 (200 micrometer deep from tangent surface of implant), the percentage of contact length was 8.6% (SD 3.9%) for the Ta controls; 13.2% (SD 4.9%) for Ta-CaP controls and 52.3% (SD 18.3%) for Ta-CaP-ALN implants. In section 2 (850 micrometer deep), the percentage contact length was 3.8% (SD

2.1%) for Ta controls; 8.1% (SD 2.8%) for Ta-CaP controls and 39.4% (SD 14.3%) for Ta-CaP-ALN implants. In section 3 (the central surface of implant), the percentage contact length was 4.6% (SD 1.4%) for Ta controls; 9.0% (SD 3.0%) for Ta-CaP controls and 40.0% (SD 17.6%) for Ta-CaP-ALN implants. The percentage of contact length of Ta-CaP-ALN implants increased by an average of 700% (8-fold) and 342% (4.42 fold) compared with those of Ta and Ta-CaP controls respectively. The average increase of contact for Ta-CaP controls was 87% (1.87-fold) compared with that of Ta controls.

The t-test results show that the enhancements of bone/implant contacts at the site of Ta-CaP-ALN samples were significant compared with Ta and Ta-CaP controls. The p-values were less than 0.0001 in both cases. Also, the increase of contact at the site of Ta-CaP controls was significant compared with Ta controls because the p-value of t-test was 0.02.

Table 5.2 The p-values of t-tests on bone/implant contacts of 3 sections

Compared groups	Section 1	Section 2	Section 3
Ta & Ta-CaP	0.02	0.0004	0.0002
Ta & Ta-CaP-ALN	<0.0001	<0.0001	<0.0001
Ta-CaP & Ta-CaP-ALN	<0.0001	<0.0001	<0.0001

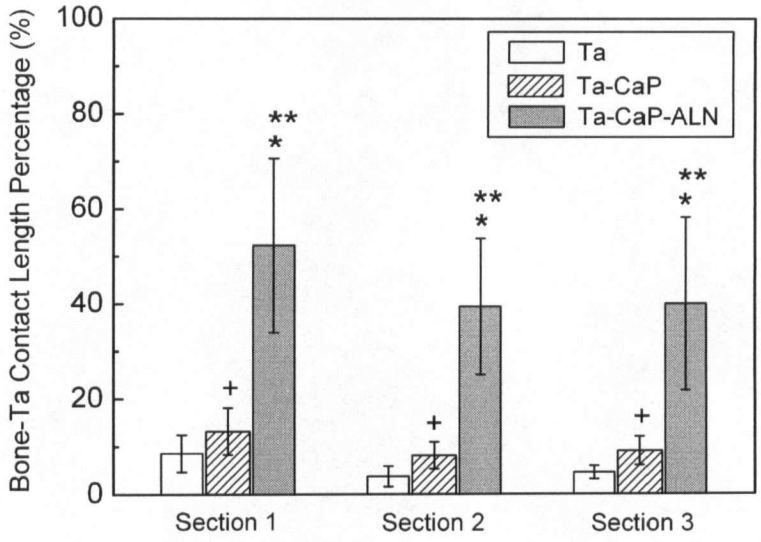

Fig. 5.9 Bone formation on the surface of porous tantalum expressed as a percentage of the available porous tantalum surface (contact length) of three sections performed through each implant. Ta-CaP-ALN demonstrated significantly increased contact length compared with Ta-CaP controls, $p < 0.0001$ *, and significantly increased contact length compared with Ta controls, $p < 0.0001$ **. Ta-CaP controls demonstrated significantly increased contact length compared with Ta controls, $p < 0.02$ +.

5.6 Bone formation mechanism

Fluorescence labeling provides the information on when and where the bone formation happens and the directions of bone growth. Base on the fluorescent images, some facts regarding the bone formation mechanism were observed and the comparison among 2 control groups and Ta-CaP-ALN implant group was conducted. Fig. 5.10 shows how the fluorescence labeling works. Fig. 5.10 (a), which is the transverse section of a tooth, shows the fluorescent rings. The growth direction can be identified by these rings with reference to the administration sequence of fluorochromes (see Table 4.4 on page 45). Fig. 5.10 (b) shows the bone initiation on a Ta-CaP control surface.

All samples (108 sections from 36 implants) revealed the new bone formation initiated at the surfaces of the host bone and bridged over the gap towards metal implants during the first 2 weeks after surgeries. This is called the distance osteogenesis [26], and the distance osteogenesis will occur regardless of the types of implants because the host bone is the best places for new bone formation.

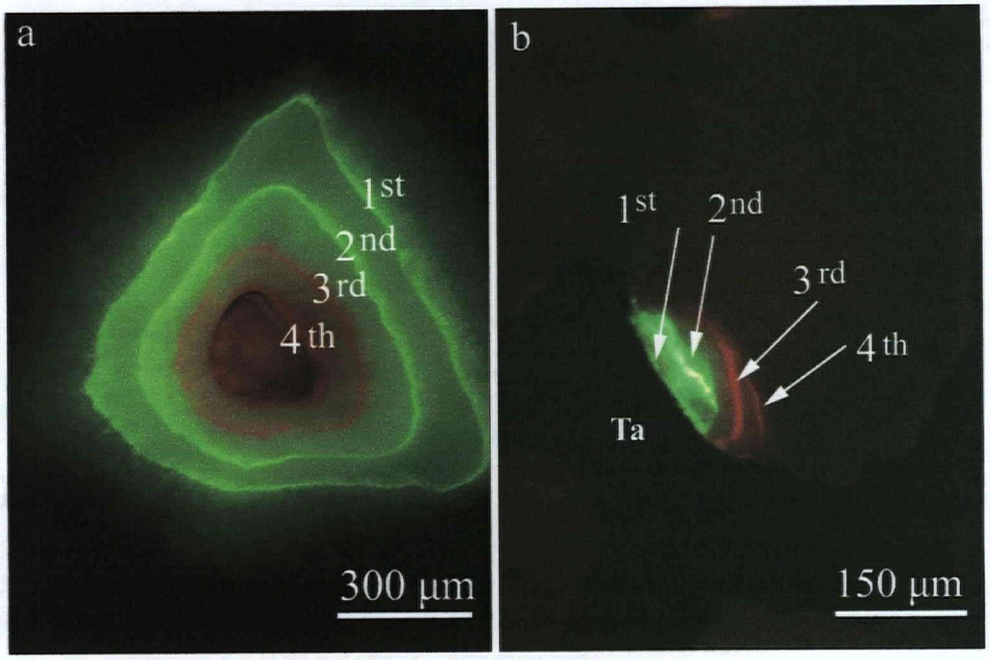

Fig. 5.10 Fluorescence images showing the labels on tooth and ingrowth bone, and the ordinal numbers gave postoperative time sequence. a) 4 color rings indicated the growth direction on tooth. The 2 green rings were calcein and 2 red rings were alizarin; b) labels indicated the bone initiation on implant surface.

The major difference between Ta-CaP-ALN implants and 2 control groups was the interaction of newly formed bone with the implant surfaces. The pattern and site of bone initiation were strongly modulated with alendronate-immobilized calcium phosphate coating. In the Ta controls, bone formation occurred inside the tantalum pores with little attachment to the surface of porous tantalum. Fig. 5.11(a) shows the bone initiation (the green lines)

occurred around the tantalum strut (not touching) and expanded (the red lines) afterward. In contrast, early bone formation on Ta-CaP-ALN plugs occurred predominantly on the surface of the tantalum struts. In Fig 5.11(b), the new bone initiation (green lines) spread on the implant surface and grew outward. Ta-CaP controls had a similar pattern of bone formation to that of the Ta controls, and bone initiation on implant surfaces was occasionally observed on the Ta-CaP controls. Fig 5.11 (c) shows similar bone initiation on a Ta-CaP control to that on a Ta control. Fig. 5.11 (d) demonstrates the bone initiation on the implant surface of a Ta-CaP control. But the initiation of bone on Ta-CaP controls was slightly different than that on the Ta-CaP-ALN implants. It only covered a portion of implant surface and expanded into pore center.

The bone ingrowth patterns were different on Ta-CaP-ALN implants from those on the two types of controls because of the change in bone formation initiation. On Ta controls (see Fig. 5.12), early bone formation occurred in the center of the porous area and expanded outwards onto the porous tantalum struts, as was tracked by the fluorescence labels (green lines were for first and second postoperative weeks, and red lines were for third and fourth weeks). The bone ingrowth went through the channel of tantalum pores and barely touched the struts. On Ta-CaP controls (see Fig. 5.13), the similar ingrowth pattern to that of Ta controls could be seen, and also a branch of bone ingrowth anchored on implant surface (Fig 5.13 (b) left bottom corner). On Ta-CaP-ALN implants (see Fig. 5.14), the bone ingrowth spread on the implant surface and followed by bone expansion towards the center of the porous channels.

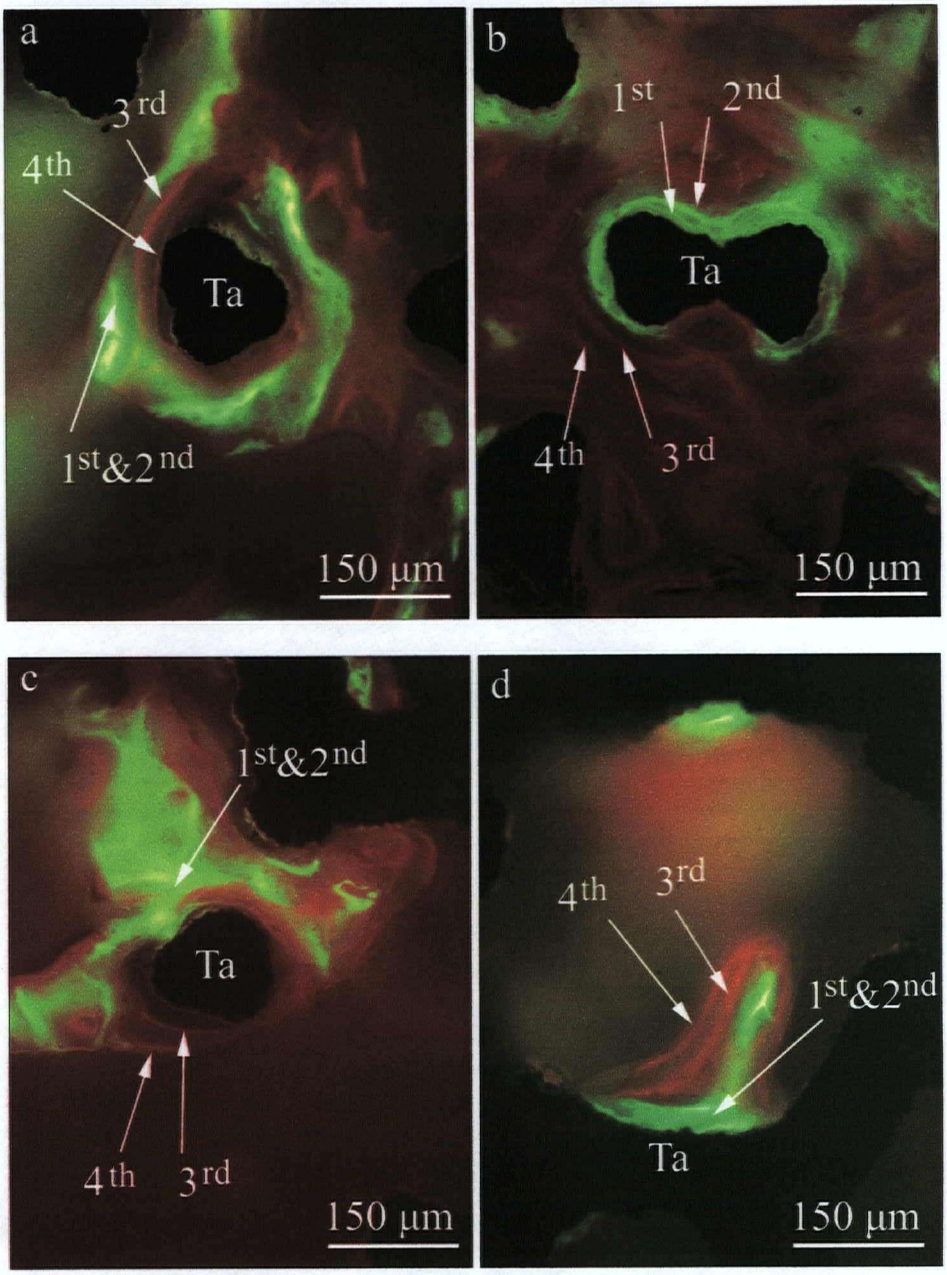

Fig. 5.11 Fluorescence images showing bone initiation. a) non-coated porous tantalum control; b) alendronate-immobilized calcium-phosphate-coated implant; c) and d)calcium-phosphate-coated controls.

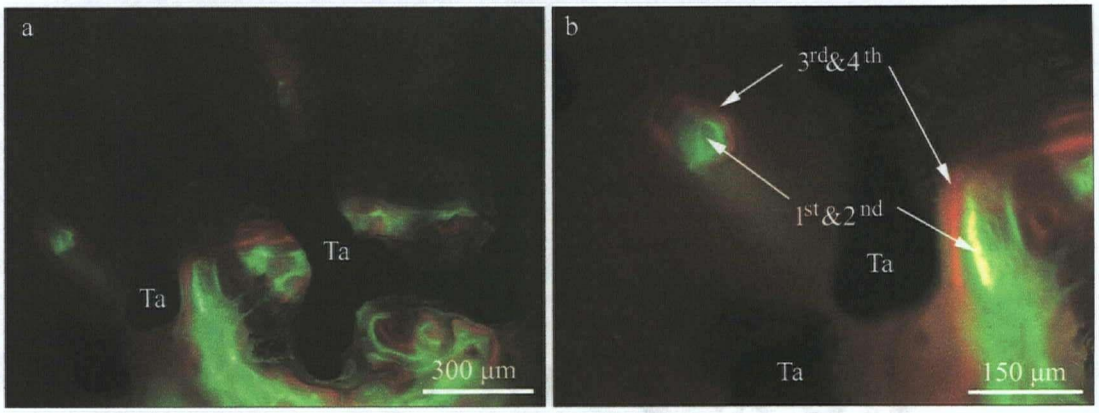

Fig. 5.12 Fluorescence images showing bone ingrowth pattern on Ta control. a) low magnification image; b) higher magnification image showing the labeling lines.

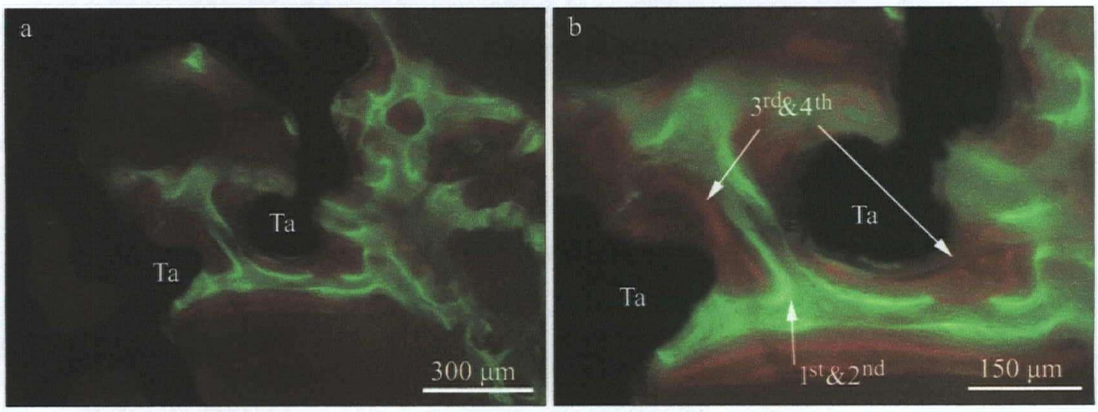

Fig. 5.13 Fluorescence images showing bone ingrowth pattern on Ta-CaP control.

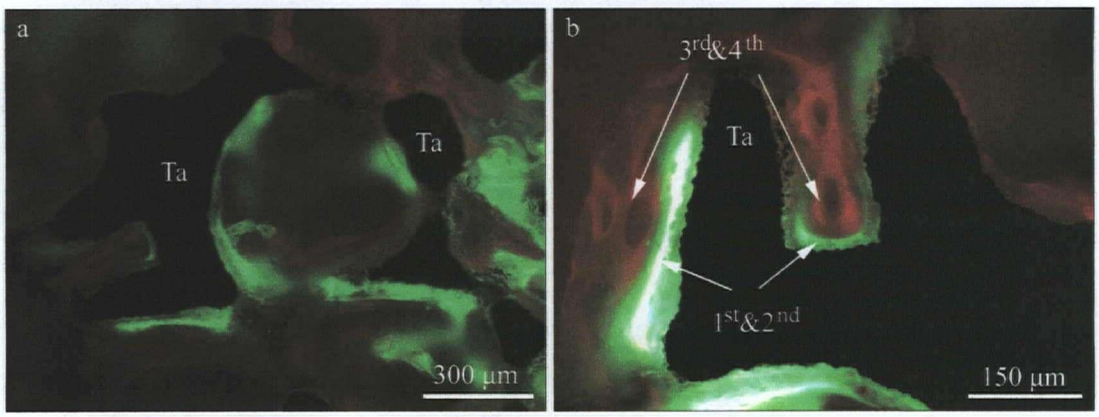

Fig. 5.14 Fluorescence images showing bone ingrowth pattern on Ta-CaP-ALN implant.

The changes in bone formation mechanism also affected the patterns of gap filling bone growth. On the Ta controls (see Fig. 5.15 (a)), new bone formation crossed over the gap area but did not anchor on the implant surface; on the Ta-CaP controls (see Fig. 5.15 (b)), there were two small portions of new bone anchored on the implant surface; on Ta-CaP-ALN implants (see Fig. 5.15 (c) and (d)), new bone fully contacted the implant surface.

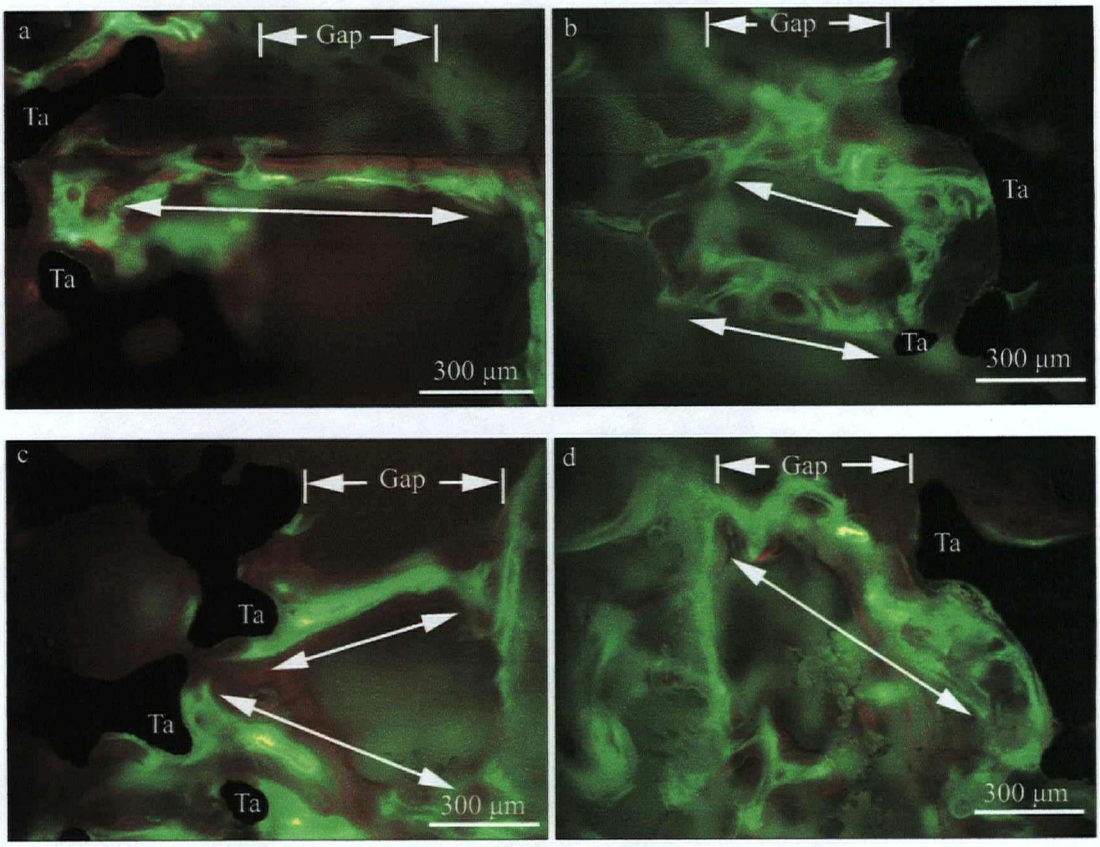

Fig. 5.15 Fluorescence images showing the bone formation at gap areas. The white lines with double arrows indicated the bone bridging gaps a) Ta control; b) Ta-CaP control; c) and d) Ta-CaP-ALN implants.

It is very important for bone/implant fixation that the new bone crossing gaps anchored on implant surfaces. Without the full bone/implant contact, there would be a possibility of micro-motion between implant and host bone. Without the bone formation

initiation on implant surface, the bone/implant integration would be postponed because the bone initiation on implant surfaces ensured a certain level of bone/implant integration in first 2 weeks postoperatively on Ta-CaP-ALN implants compared with bone still barely touching the implant surfaces 4 weeks after the surgeries on the Ta controls.

CHAPTER 6: DISCUSSION

6.1 The effects of calcium phosphate coating

Hydroxyapatite is a bioactive ceramic. Many reports on hydroxyapatite enhancing bone formation were published [90, 91,92]. Barrére et al [93] claimed that biomimatic coating of OCP increased the osteoinductivity (defined on page 12) of porous tantalum when implant locations were inside the back muscles goats, and he could not fully claim the increase of osteoinductivity by biomimatic coated OCP when the porous tantalums were implanted in distal femur. Davies JE [23] believed the BMP might adsorb on porous-structure hydroxyapatite and therefore enhance osteoinduction. However, with a gap existing between implants and host bone, our animal tests did not reveal significant increase of peri-prosthetic bone formation. Although there were 21.5% and 38.3% increases of gap filling and ingrowth respectively, the p-values of t-tests were 0.12 and 0.07 respectively. Therefore, the osteoinductivity of porous tantalum implants was not significantly increased by calcium phosphate coating process when challenging bone/implant gaps and defects.

Despite the weak effects on the osteoinductivity of implants, the calcium phosphate coating significantly increased the new bone-formation/implant contacts. Our testing results showed an average of 87% (1.87-fold) increase of contact lengths on Ta-CaP implants compared with those on Ta controls. With the help of fluorescence images, the initiation of new bone formation on the strut surfaces, which was also called contact osteogenesis, was occasionally observed on Ta-CaP implants compared with little bone initiation on implant

surfaces of Ta control. These results provided the direct evidences and explanations to why bone/implant contacts were increased by calcium phosphate coating process.

The initiation of new bone formation on calcium phosphate coating surfaces indicated better attachment of osteoblasts and osteogeneritor cells. In another words, the calcium phosphate coating process increased the osteoconductivity (defined on page 12) of porous tantalum implants. Theoretically, the increase of bone /implant contact may contribute to the eventual implant fixation.

Summer et al [46] reported that the hydroxyapatite-tricalcium phosphate coating did not contribute to fixation, bone ingrowth, and bone formation based on their mechanical testing and histomorphometry results of a gap model animal test on BMP treated implants. They analyzed the fixation strength, interface stiffness and energy to failure and found no difference with or without hydroxyapatite-tricalcium phosphate coatings. They also analyzed the bone volume, trabecular numbers and trabecular plate thickness etc on both calcium phosphate coated samples and the controls. They found no difference either. Their results supported our findings.

In conclusion, in the presence of a gap between bone and the implant, our ELD calcium phosphate coating increases the bioactivity of porous tantalum implants in terms of osteoconductivity. The testing results show evidence of better osteoconductivity and contact osteogenesis on calcium phosphate coating surfaces compared with non-coated tantalum surfaces. However, the calcium phosphate coating treatment did not significantly change the

osteoinductivity of porous tantalum, and therefore the peri-prosthetic new bone formation was not increased. As a result, the bone/implant fixation might not be obviously improved by calcium phosphate coating process.

6.2 The effects of alendronate-immobilized calcium phosphate coatings

Our gap model study demonstrated a significant enhancement of bone ingrowth (19.9 % versus 6.0%), bone gap filling (29.1% versus 13.0%) and total bone formation (26.2 % versus 9.7%) associated with Ta-CaP-ALN samples compared with Ta controls. At the same time, an alendronate surface treatment significantly enhanced bone ingrowth (140 %; 2.40-fold), gap filling (84%; 1.84-fold) and total bone formation (111%; 2.11-fold) in comparison with Ta-CaP controls.

Possible explanations of the enhancement of bone formation towards implants could be: the effects of alendronate on bone cells increased the activities of osteoblasts work and decreased the activities of osteoclasts; or the alendronate-immobilized calcium phosphate coating increased osteoinductivity of porous tantalum which meant more stem cells differentiated to osteoblasts. Davies JE [23] believed the osteoblasts would be trapped in bone and became osteocytes after the mineralization of the bone matrix. For further bone growth, new osteoblasts needed to be recruited. In order to clearly understand the mechanism behind the enhancement of new bone formation, further studies need to be conducted.

The histomorphometry analysis also showed that the alendronate-immobilized calcium phosphate coating significantly increased bone/implant contacts compared with Ta-

CaP controls (342%; 4.42-fold) and Ta controls (700%; 8-fold). The fluorescence imaging found that the initiation of bone formation happened on the implant surface throughout the Ta-CaP-ALN implants. The osteoconductivity of these implants was therefore dramatically increased compared with both Ta-CaP and Ta controls. The significant increase of contact osteogenesis on alendronate-immobilized calcium phosphate coating indicated that it was the best bioactive implant surface out of the three types of implants.

The XRD, FTIR and SEM imaging analysis of coatings revealed no changes on morphology and crystal structure of the ELD calcium phosphate coating after alendronate immobilization. This eliminated any other potential factors, such as a change in the crystal structure of calcium phosphate from OCP to HA, that happened and affected the bioactivity of the coating surfaces. Therefore, the dramatic enhancements of bone formation and osteoconductivity of porous tantalum implants were essentially due to the presence of alendronate.

The results of our study are also consistent with recent in vivo tests reported in the literature. The effect of zoledronate on bone ingrowth into porous tantalum implants was studied in a canine model by a single post-operative intravenous injection [67]. Subsequently, zoledronate was bound to hydroxyapatite-coated porous tantalum, and an increase of 134% in bone ingrowth was reported by the same group [68]. In our gap model with a less potent bisphosphonate (alendronate), however, we found a greater relative increase in bone ingrowth compared with the zoledronate study (232% versus 134%) [68].

The differences in our findings may be related to several factors including differences in animal models, the type of bisphosphonate used, length of implantation, location of implantation and the design of the implants. Another key difference between our study and previous studies is the unique micro-porous calcium phosphate coating made by ELD technique. Such a coating may not significantly affect bone formation itself, but it acts as a very effective carrier for bisphosphonate delivery.

Because of the effects of alendronate-immobilized calcium phosphate coating on osteoconductivity of porous tantalum implants, bone reaction to implants was completely changed, and the initiation of bone formation happened on the surface of the alendronate-immobilized calcium phosphate coatings. In addition, alendronate-immobilized calcium phosphate coating increased new bone formation towards implants. As a result, more bone formed bridging the gap between host bone and implant and anchored onto the implant surface, and eventually better bone/implant fixation could be achieved.

6.3 Clinical relevance of the gap model animal tests and alendronate delivery implants

It has been known that biological fixation of porous implants occurs by micro-interlocking with ingrown tissue. Autopsy studies have demonstrated that bone ingrowth occurs in only 30-40% of the surface area of the implant in primary total hip arthroplasty [94]. In revision hip arthroplasties, bone defects and gaps may significantly compromise the quantity and quality of host bone available for ingrowth. In many cases less than 50% host

bone is available for bone ingrowth of the newly implanted shell. Therefore, any solutions to achieve a reliable and durable bone ingrowth to porous materials would potentially lead to novel implants for challenging revision cases.

Gaps and defects that occur between the surface of the implant and the host bone in an acetabular reconstruction are usually filled with bone graft or bone graft substitutes in current clinical practice. However, bone ingrowth into porous implants is poor in the presence of acetabular defects, regardless of the defect filling with bone graft. In an earlier study, acetabular defects were created in a canine model which were left unfilled or were filled with either autograft bone or a 50:50 mixture of autogenous bone graft and hydroxyapatite/tricalcium phosphate (HA/TCP) ceramic [95]. At 6 weeks post operation, grafting improved defect healing but had inferior bone ingrowth compared with empty defects.

In our study, a rabbit implant model incorporating a gap between porous tantalum and bone was developed to assess the effect of alendronate coated porous tantalum compared against the controls. The model sought to replicate the clinical scenario in total hip revision arthroplasty. Implantation of the plugs in the metaphyseal region also closely replicates the clinical scenario in that the implants were placed in cancellous bone. The positive results of our study indicate that the surface treatment technique could provide an effective solution to the clinical challenges discussed above. Another application is the spinal fixation where fast and more bone ingrowth to the implants are critical to the function.

6.4 Key progresses in ELD surface drug delivery and animal studies

A unique technique in this study is the electrolytic deposition and the resulting micro-porous calcium phosphate coating. The calcium phosphate coating itself does not seem to have significant impact on bone growth. This relative uniform calcium phosphate coating, however, provides an ideal surface carrier for bisphosphonate local delivery. The electrolytic deposition used in this study has obvious advantages over plasma spray and biomimetic coating for porous Ta implants. In plasma spray, only a half thickness of the porous cells on Ta implant surface can be coated with calcium phosphate because of the line-of-sight limitation. As a result, bone ingrowth into deeper porous area can not be improved. Biomimetic coating technique is a relatively slow process. It requires careful surface pre-treatment and strict control over the solution conditions. The calcium phosphate coatings tend to form spherulites. Electrolytic deposition with periodical stirring could make a relative uniform and porous coating both inside and on the surface of the porous Ta implants.

Another unique feature of our animal tests is the introduction of fluorochrome injections to the bone formation mechanism studies. The fluorochromes mark the front of bone formation, and many people have used a series of fluorochromes to reveal bone growth direction and growth speeds etc. We employed this fluorescence technique to examine the mechanism of bone formation on different types of surfaces of porous tantalum implants and visualize the initiation of bone formation on the surface of alendronate-immobilized calcium phosphate coating.

Alendronate-immobilized calcium phosphate coating provides an advanced drug delivery method that can directly send alendronate to symptom location. It dramatically reduces the drug dose without compromising any healing effects. Also, alendronate, as one of bisphosphonates, has many advantages over many other materials such as hydroxyapatite and BMP. Other methods of augmenting the rate and extent of bone ingrowth into porous implants have been described in the literature, including the use of BMP [46, 96], Bone-like Carbonated Apatitic (BCA) coating [93], bone matrix gel [97] and non invasive low intensity ultrasound [98]. The advantage of bisphosphonates over BMP is their relatively low cost. Other advantages of bisphosphonates are their established clinical record, their effects on reducing bone resorption thereby decreasing stress shielding [99] and wear particle-induced osteolysis [41].

Improvements to the design and biomaterial properties of any drug-implant delivery system can only be made by understanding the principles underlying the mechanism of action of the drug- delivery system. The mechanism of enhanced bone ingrowth and osteoconductivity of Ta-CaP-ALN provides further insight into the underlying action of this drug delivery system. Enhancement of bone ingrowth, gap filling and increased osteoconductivity of Ta-CaP-ALN could have very significant advantages in revision joint arthroplasties associated with host bone defects, providing early and enhanced biological fixation in complex cases.

CHAPTER 7: CONCLUSIONS

A gap model animal test was designed and successfully conducted to study the effects of alendronate-immobilized calcium phosphate coatings on bone formation towards porous tantalum implant. The gap model imitated the clinical scenario. This and other unique features, such as the porous ELD coatings of calcium phosphate, alendronate immobilization and fluorescence labeling etc, distinguished this animal test from any others and represented significant improvements in implant/bone interaction study. Following are the main conclusions drawn from this animal test:

1. Alendronate-immobilized calcium phosphate coating enhanced the bone formaton towards porous tantalum implants. The treatment could significantly accelerate early stage (4 weeks) bone growth (by170%) as compared with porous Ta by itself. The increase was 111% when compared with Ta-CaP controls. Although Ta-CaP implant increased total bone formation by 28%, the improvement was not statistically significant.

2. Both calcium phosphate coatings before and after alendronate immobilization significantly increased the osteoconductivity of porous tantalum implants. Alendronate immobilized calcium phosphate coating achieved much greater enhancement. Alendronate immobilization treatment demonstrated dramatic and significant increase in bone/Tantalum contact. As compared with porous tantalum itself, Ta-CaP-ALN implant increased bone coverage on tantalum by 770%. The increase was 344% when compared with Ta-CaP controls. Calcium phosphate

coating increased the bone/implant contact length by 87% compared with Ta controls.

3. The observation of fluorescence labeling images showed that the treatment of alendronate-immobilized ELD-coating of calcium phosphate changed the new bone formation mechanism. New bone formation initiated on the Ta-CaP-ALN surfaces, and this provided the explanation why new bone/implant contacts increased on Ta-CaP-ALN implants.

4. Early bone/implant integration may be achieved on Ta-CaP-ALN implants. The fluorescence images showed that new bone crossing gaps anchored on the implant surface in the first two weeks postoperatively.

5. Alendronate-immobilized calcium phosphate coating on porous tantalum has advantages in overcoming the gaps between the bone and the implant, and the surface design can be potentially employed to solve some of the clinical issues associated with revision surgery.

CHAPTER 8: RECOMMENDATION FOR FUTURE WORK

This animal test provided very promising results on the enhancements of osteoconduction and bone ingrowth on porous tantalum by alendronate-immobilized calcium phosphate coating. It is a technique that has potential clinical applications. Before any clinical trial could be discussed, the following experiments need to be conducted for further confirmation of the results.

1. Systematic study on the effect of alendronate loading amounts to optimize the drug dosage and to achieve the best effects on bone/implant fixation.

2. More in depth study on the mechanisms of how alendronate immobilized calcium coating enhances osteoconductivity and new bone formation towards porous tantalum implants.

3. Design and launch the mechanical tests to collect data on the bone/implant fixation. Furthermore, confirm the enhancement of bone/implant fixation on alendronate immobilized calcium phosphate coated implants.

4. Systematic study of new bone/implant fixation against varying postoperative ingrowth time.

REFERENCES

1. Just what is osteoporosis? Retrieved on Feb. 25th, 2007 from A women's perspective website:http://www.cumc.columbia.edu/dept/partnership/newsletters/volume1_Issuse 2/osteoporosis.html

2. You can be strong and vulnerable at the same time. Retrieved on Feb. 25th, 2007 from WebMD website: http://www.webmd.com/solutions/osteoporosis-risks/strong-vulnerable

3. Hospital Morbidity Database, CIHI, 1994–1995 and 2004–2005.

4. Freeman MA et al. Early migration and late aseptic failure of proximal femoral prostheses. J Bone Joint Surg Br 1994; 76(3): 432-438.

5. Maloney WJ et al. Fixation, polyethylene wear, and pelvic osteolysis in primary total hip replacement. Clin Orthop Rel Res 1999; 369:157-164.

6. Duncan CP et al. Editorial-Antibiotic Depots. J Bone Joint Surg Am 1993; 75-B (3):349-350.

7. Meraw SJ et al. Qualitative analysis of peripheral peri-implant bone and influence of alendronate sodium on early bone regeneration. J Peridontol 1999;70:1228-1233.

8. Tengvall P et al. Surface immobilized bisphosphonate improves stainless-steel screw fixation in rats. Biomaterials 2004; 25: 2133-2138.

9. Yoshinari M et al. Bone response to calcium phosphate-coated and bisphosphonate immobilized titanium implants. Biomaterials 2002; 23: 2879-2885,

10. Li EC et al. Zoledronic acid: A new parenteral bisphosphonate. Clin Ther 2003; 25: 2669-2708.

11. Hoffman AA et al. Comparative study of human cancellous bone remodeling to titanium and hydroxapatite coated implants. J Arthroplasty 1993; 8:157-66.

12. Charnley J. Arthroplasty of the hip – a new operation. Lancet 1961; 277(7187): 1129-1132.

13. Baier RE. Surface behaviour of biomaterials: The theta surface for biocompatibility. J Mater Sci Mater Med 2006; 7(11):1057-62.

14. Bobyn JD et al. Clinical validation of a structural porous tantalum biomaterial for adult reconstruction. J Bone and Joint Surg. 2004; 86(A) supplement 2: 123-129.

15. Curry JD. The Mechanical Adaptations of Bones. First edition; Princeton Univ. Press. NJ USA 1984; 24 -37

16. Weiner S et al. The Material Bone: Structure-Mechanical Function Relations. Annu Rev Mater Sci 1998; 28: 271-298

17. Rho J et al. Mechanical properties and the hierarchical structure of bone. Med Eng Phys 1998; 20 (2): 92 – 102

18. Lowenstam HA et al. On Biomineralization. Oxford Univ. Press, Oxford, UK 1989

19. Mann S et al. Biomineralization: Structural question at all length scale. J struct Bio 1999; 126(3): 179-181.

20. Currey JD. What determines the bending strength of compact bone? J Exp Biology 1999; 202: 2495-2503.

21. Weiner S et al. Lamellar bone: Structure-function relations. J Struct Biology 1999; 126: 241- 255

22. Ryland BE et al. Histologic Analysis of Bone Healing. In: An YH, Martin KL, eds. Handbook of Histology Methods for Bone and Cartilage, Humana Press, Totowa, New Jersey USA 2003; chapter.28; 375–390.

23. Davies JE. Understanding peri-implant endosseous healing. J of Dental Edu 2003; 67(8): 923-949

24. Davies JE. In vitro modeling of the bone/implant interface. Anat Rec 1996;245:426-445

25. Dimitriou R et al. Current concepts of molecular aspects of bone healing. Injury 2005; 36: 1392-1404.

26. Neuhoff D DVM et al. Anodic Plasma Chemical Treatment of Titanium Schanz Screws Reduces Pin Loosening. J Orthop Trauma 2005; 19(8): 543-550.

27. Park JB et al. Metallic Biomaterials. In Park JB et al. Biomaterials: principles and applications. CRC Press, Boca Raton 2003; Chapter 1: 1-20

28. Muratoglu OK et al. Alternate bearing surfaces in hip replacement In: Sinha RK editor. Hip replacements: current trends and controversies. New York: Marcel Dekker, 2002. p. 1-46.

29. Firkins PJ, et al. Quantitative analysis of wear and wear debris from metal-on-metal hip prostheses tested in a physiological hip joint simulator. Biomed Mater Eng 2001; 11: 143-157.

30. Galea G et al. Review article: Clinical effectiveness of processed and unprocessed bone. Transfusion Medicine 2005; 3: 165-174.

31. Bobyn JD et al. Characteristics of bone ingrowth and interface mechanics of a new porous tantalum biomaterial. J Bone Joint Surg 1999; 81B: 907-914.

32. Tsao AK et al. Biomechanical and clinical evaluations of a porous tantalum implant for the treatment of early-stage osteonecrosis. J of Bone & Joint Surg Am 2005; 87: 22-27.

33. Matsuno H et al. Biocompatibility and osteogenesis of refractory metal implants, titanium, hafnium, niobium, tantalum and rhenium. Biomaterials 2001; 22:1253-1262.

34. Bobyn JD et al. Tissue response to porous tantalum acetabular cups, a canine model. J of Arthroplasty 1999; 14 (3): 347-354.

35. Bobyn JD et al. Fundamental principles of biologic fixation. In: Morrey BF,ed. Reconstructive surgery of the joints. New York, etc: Churchill Livingstone 1996. p. 75-94,

36. Sabokbar A et al. Bisphosphonates in bone cement inhibit PMMA particle induced bone resorption. Ann Rheum Dis 1998; 57: 614-618.

37. Schwarz EM et al. Quantitative small-animal surrogate to evaluate drug efficacy in preventin wear debris-induced osteolysis. J Orthop Res 2000; 18: 849-855.

38. Total hip replacement: What it is. How it helps. Retrieved on Dec 21st, 2006 from Anderson orthopaedic research institute website: http://www.aori.org/thr/thrwhat.html

39. Moorhouse J. Waiting game. Retrived on Dec 20th, 2006 from Canadian health care manager website: http://www.chmonline.ca/issue/article.jsp=20020201_210080_9280

40. Horowitz SM et al. Phamacologic inhibition of particulate-induced bone resorption. J Biomed Mater Res 1996; 31: 91-96.

41. Shanbhag AS et al. Inhibition of wear debri mediated osteolysis in a canine total hip arthroplasty model. Clin Orthop Relat Res 1997; 344: 33-43.

42. McGrory et al.: Effect of femoral offset on range of motion and abductor muscle strength after total hip arthroplasty. J Bone Joint Surg Br 1995; 77-B(6): 865-9

43. Pennock J.et al. Morse type tapers. J Arthroplasty 2002; 17: 773-8

44. Rosenberg AG. Cementless acetabular components: the gold standard for socket revision. J Arthroplasty 2003; 18 (No.3 Suppl 1): 118-20.

45. Cohen R. A porous tantalum trabecular metal: basic science. Am J Orthop 2002; 31(4):216-7.

46. Sumner DR et al. Locally delivered rhBMP-2 enhances bone ingrowth and gap healing in a canine model. J Orthop Res 2004; 22:58- 65.

47. Sumner DR et al. Enhancement of bone ingrowth by transforming growth factor-beta. J of Bone and Joint Surg Am. 1995; 77-A (8): 1135-1147.

48. Sunmer DR et al. Additive enhancement of implant fixation following combined treatment with RH TGF-β2 and RH BMP-2 in a canine model. J Bone Joint Surg 2006; 88-A (4): 806-817.

49. LeGeros RZ. Calcium phosphate materials in restorative dentistry: A review. Adv Dent Res 1988; 2(1): 164-180

50. Koutsoukos P et al. Crystallization of calcium phosphates-constant composition study. J Am Chem Soc 1980; 102: 1553 -1557

51. Ducheyne P et al. The effect of calcium phosphate ceramic composition and structure on in vitro behavior. 1. Dissolution. J biomed mater res 1993; 27: 25-34.

52. Shi SL et al. Reinforcement of hydroxyapatite bioceramic by addition of Ti_3SiC_2. J Am Ceram Soc 2006; 89: 743-745.

53. Tsui YC et al. Plasma sprayed hydroxyapatite coatings on titanium substrates Part 1: Mechanical properties and residual stress levels. Biomaterials 1998; 19: 2015-2029

54. Sun LM et al. Material fundamentals and clinical performance of plasma-sprayed hydroxyapatite coatings: A review. J of Biomed Mater Res 2001; 58: 570-592

55. Gross KA et al. Amorphous phase formation in plasma sprayed hydroxyapatite coatings. J of Biomed Mater Res 1998; 39: 407-414

56. Cui FZ et al. Preparation of calcium phosphate coating on porous tantalum. J of Mater Sci Letter 1998; 17: 925-930.

57. Compbell AA et al. Surface-induced mineralization: A new method for producing calcium phosphate coatings. J Biomed. Mater. Res. 1996; 32: 111–118.

58. Liu Q et al. The role of surface functional groups in calcium phosphate nucleation on titanium foil: a self-assembled monolayer technique. Biomaterials 2002; 23: 3103–3111.

59. Duan K et al. Surface modifications of bone implants through wet chemistry. J. Mater. Chem. 2006; 16: 2309 – 2321.

60. Zhitomirsky I. Cathodic electrodeposition of ceramic and organoceramic materials. Fundamental aspects. Adv Colloid Interface Sci 2002; 97: 277–315.

61. Duan K et al. Electrochemical deposition and patterning of calcium phosphate bioceramic coatings. Ceramic Trans 2003; 47: 53-61.

62. Fleisch H. Bisphosphonates in bone disease: from the laboratory to the patient. 4th edition. San Diego: Academic Press, 2000.

63. Sabokbar A et al. Bisphosphonates in bone cement inhibit PMMA particle induced bone resorption. Ann Rheum Dis 1998; 57: 614-618.

64. Schwarz EM et al. Quantitative small-animal surrogate to evaluate drug efficacy in preventing wear debris-induced osteolysis. J Orthop Res 2000; 18: 849-855.

65. Horowitz SM et al. Phamacologic inhibition of particulate-induced bone resorption. J Biomed Mater Res 1996; 31: 91-96.

66. Lin JH et al. Physiological disposition of alendronate, a potent anti-osteolytic bisphosphonate, in laboratory animals. Drug Metabolism and Disposition 1991 19; 926-932

67. Bobyn JD et al. Zoledronic acid causes enhancement of bone growth into porous implants. J Bone Joint Surg Br 2005; 87B: 416-20.

68. Tanzer M et al. Bone augmentation around and within porous tantalum implants by local bisphosphonate elution. Clin Orthop Relat Res 2005; 441: 30-39.

69. Peter B et al. Local delivery of bisphosphonate from coated orthopaedic implants increases implants mechanical stability in osteoporotic rats. J Biomed Mater Res 2006; 76A: 133-143

70. Binderman I et al. Effectiveness of local delivery of alendronate in reducing alveolar bone loss fellowing periodontal surgery in rats. J Periodontal 2000; 71(8): 1236-40.

71. Della Valle CJ et al. Revision of the acetabular component without cement after total hip arthroplasty. A concise follow-up, at fifteen to nineteen years, of a previous report. J Bone Joint Surg Am 2005; 87(8): 1795-800.

72. Zhang YD et al. Interfacial frictional behavior: Cancellous bone cortical bone and a novel porous tantalum biomaterial. J Musculoskeletal Res 1999; 3: 245-251

73. Kold S et al. Bone /compaction enhances fixation of hydroxyapatite-coated implants in a canine gap model. J Biomed Mater Res Part B: Appl Biomater 2005; 75B: 49–55.

74. Erben RG Bone-labeling technique. In: An YH, Martin KL, eds. Handbook of Histology Methods for Bone and Cartilage, Humana Press, Totowa, New Jersey USA 2003; chapter.5; 99-117.

75. Urist MR et al. Chemical reactivity of mineralized tissue with oxytetracycline. Arch of Pathol 1963; 76: 484-496

76. Jansen JA Histological analysis of bone-implant interface. In: An YH, Martin KL, eds. Handbook of Histology Methods for Bone and Cartilage, Humana Press, Totowa, New Jersey USA 2003; chapter.26; 353-360.

77. Pautke C et al. Polychrome labeling of bone with seven different fluorochromes: Enhancing fluorochrome discrimination by spectral image analysis. Bone 2005; 37: 441 – 445.

78. Frosch KH et al. Autologous osteoblasts enhance osseointegration of porous titanium implants. J of Orthop Res 2003; 21: 213 -223.

79. Altman DG. Practical statistics for medical research. Chapman and Hall/CRC Press, Boca Raton, Florida USA 1990

80. Paulson DS. Applied statistical designs for the researcher. Marcel Dekker, Inc., New York, New York USA 2003

81. Medical terminology and drug database. Retrieved on March 2nd, 2007 from St. Jude children's research hospital website: http://www.stjude.org/legal/0,262588_3170. htm

82. Deacon J. Student's t-test. Retrieved on Feb 25th, 2007 from the University of Edinburgh website: http:// helios.bto.ed.ac.uk/bto/statistics/tress4a.html

83. Dziewiatkowski DD. Isolation of chondroitin sulphate-^{35}S from articular cartilage of rats. J. Biol. Chem. 1951; 189: 187-190

84. Bauer JH. Oral administration of radioactive sulphate to measure extracellular fluid space in man. J. Appl. Physiol. 1976; 40: 1976.

85. Bauer TW et al. Cutting and Grinding Methods for Hard-Tissue Histology. In: An YH, Martin KL, eds. Handbook of Histology Methods for Bone and Cartilage, Humana Press, Totowa, New Jersey USA 2003; chapter.15; 233– 242.

86. Bergstrom JD et al. Alendronate is a specific, nanomolar inhibitor of farnesyl diphosphate synthase. Arch Biochem Biophys 2000; 373(1):231-41

87. Wang J et al. Biomimetic and electrolytic calcium phosphate coatings on titanium alloy: physicochemical characteristics and cell attachment. Biomaterials 2004; 25: 583–92.

88. Fowler OB et al. Octacalcium phosphate. 3.Infrared and Raman vibrational spectra. Chem Mater 1993; 5: 1417–23.

89. Duan K. PhD thesis. The University of British Columbia. Vancouver, BC. Canada 2007

90. Suchanek W et al. Processing and properties of hydroxyapatite-based biomaterials for use as hard tissue replacement implants. J Mater Res 1998; 13: 94-117

91. Willmann G. Coating of implants with hydroxyapatite material connections between bone and metal. Adv Eng Mater 1999; 1: 95-105

92. Chang YL et al. Calcium and phosphate supplementation promotes bone cell mineralization: Implications for hydroxyapatite (HA)-enhanced bone formation. J Biomed Mater Res. 2000; 52: 270-278

93. Barrére F et al. Osteointegration of biomimetic apatite coating applied onto dense and porous metal implants in femurs of goats. J Biomed Mater Res 2003; 67B(1): 655-65.

94. Pidhorz LE et al. A quantitative study of bone and soft tissues in cementless porous-coated acetabular components retrieved at autopsy. J Arthroplasty 1993; 8: 213-225.

95. Kang JD et al. Ingrowth and formation of bone in defects in an uncemented fiber-metal total hip-replacement model in dogs. J Bone Joint Surg 73A:93- 105, 1991.

96. Barrack RL et al. Induction of bone ingrowth from an acetabular defect to a porous surface with osteogenic protein-1. Clin Orthop Relat Res 2003; 417: 41-9.

97. Cook SD et al. The effect of demineralized bone matrix gel on bone ingrowth and fixation of porous implants. J Arthroplasty 17:402-408, 2002.

98. Tanzer M et al. Enhancement of bone growth into porous intramedullary implants using non-invasive low intensity ultrasound. J Arthroplasty 2002; 19:195-199.

99. Wilkinson JM et al. Effect of pamidronate in preventing local bone loss after total hip arthroplasty: a randomized, double-blind, controlled trial. J Bone Miner Res 2001; 16: 556-64.

APPENDICES

Appendix A: Student's t table (reprinted from ref 82 courtesy of Deacon J.)

Degrees of Freedom	Probability, *p*			
	0.1	**0.05**	**0.01**	**0.001**
1	6.31	12.71	63.66	636.62
2	2.92	4.30	9.93	31.60
3	2.35	3.18	5.84	12.92
4	2.13	2.78	4.60	8.61
5	2.02	2.57	4.03	6.87
6	1.94	2.45	3.71	5.96
7	1.89	2.37	3.50	5.41
8	1.86	2.31	3.36	5.04
9	1.83	2.26	3.25	4.78
10	1.81	2.23	3.17	4.59
11	1.80	2.20	3.11	4.44
12	1.78	2.18	3.06	4.32
13	1.77	2.16	3.01	4.22
14	1.76	2.14	2.98	4.14
15	1.75	2.13	2.95	4.07
16	1.75	2.12	2.92	4.02
17	1.74	2.11	2.90	3.97
18	1.73	2.10	2.88	3.92
19	1.73	2.09	2.86	3.88
20	1.72	2.09	2.85	3.85
21	1.72	2.08	2.83	3.82
22	1.72	2.07	2.82	3.79
23	1.71	2.07	2.82	3.77
24	1.71	2.06	2.80	3.75
25	1.71	2.06	2.79	3.73
26	1.71	2.06	2.78	3.71

27	1.70	2.05	2.77	3.69
28	1.70	2.05	2.76	3.67
29	1.70	2.05	2.76	3.66
30	1.70	2.04	2.75	3.65
60	1.67	2.00	2.66	3.46
120	1.66	1.98	2.62	3.37
∞	1.65	1.96	2.58	3.29